JCTC Journal of Chemical Theory and Computation

ARTICLE

pubs.acs.org/JCTC

Multiconfigurational Second-Order Perturbation Theory Restricted Active Space (RASPT2) Studies on Mononuclear First-Row Transition-Metal Systems

Steven Vancoillie, Hailiang Zhao, Van Tan Tran, Marc F. A. Hendrickx, and Kristine Pierloot*

Department of Chemistry, University of Leuven, Celestijnenlaan 200F, B-3001 Heverlee, Belgium

Supporting Information

ABSTRACT: A series of model transition-metal complexes, CrF_6, ferrocene, $Cr(CO)_6$, ferrous porphin, cobalt corrole, and FeO/FeO^-, have been studied using second-order perturbation theory based on a restricted active space self-consistent field reference wave function (RASPT2). Several important properties (structures, relative energies of different structural minima, binding energies, spin state energetics, and electronic excitation energies) were investigated. A systematic investigation was performed on the effect of: (a) the size and composition of the global RAS space, (b) different (RAS1/RAS2/RAS3) subpartitions of the global RAS space, and (c) different excitation levels (out of RAS1/into RAS3) within the RAS space. Calculations with active spaces, including up to 35 orbitals, are presented. The results obtained with smaller active spaces (up to 16 orbitals) were compared to previous and current results obtained with a complete active space self-consistent field reference wave function (CASPT2). Higly accurate RASPT2 results were obtained for the heterolytic binding energy of ferrocene and for the electronic spectrum of $Cr(CO)_6$, with errors within chemical accuracy. For ferrous porphyrin the intermediate spin $^3A_{2g}$ ground state is (for the first time with a wave function-based method) correctly predicted, while its high magnetic moment ($4.4\,\mu_B$) is attributed to spin−orbit coupling with very close-lying $^5A_{1g}$ and ^3E_g states. The toughest case met in this work is cobalt corrole, for which we studied the relative energy of several low-lying Co(II)−corrole π radical states with respect to the Co(III) ground state. Very large RAS spaces (25−33 orbitals) are required for this system, making compromises on the size of RAS2 and/or the excitation level unavoidable, thus increasing the uncertainty of the RASPT2 results by 0.1−0.2 eV. Still, also for this system, the RASPT2 method is shown to provide distinct improvements over CASPT2, by overcoming the strict limitations in the size of the active space inherent to the latter method.

1. INTRODUCTION

Multiconfigurational perturbation theory based on a complete active space reference wave function (CASSCF/CASPT2)[1,2] is a well-established computational quantum chemistry method for the study of relatively large transition-metal (TM) complexes, for which it is often seen as a preeminent wave function-based 'alternative' to density functional theory (DFT).[3] The recent possibility of using multiconfigurational second-order perturbation theory based on a restricted active space reference wave function (RASSCF/RASPT2), instead of a complete active space reference wave function, has significantly reduced the computational cost associated with large active spaces.[4] This has already lead to a number of publications either to test how this new method can be used to achieve similar accuracy, while reducing the calculation time,[5−7] and to overcome the size limitations of the active space in case of multicenter TM complexes,[4] oligomeric hydrocarbons,[8] and TMs bonded to extended π systems.[9,10]

In a recent paper of Sauri et al.,[6] several computational strategies were introduced for selecting and dividing the RASSCF/RASPT2 active space. This is more difficult than for the CASSCF/CASPT2 method because of the number of possible divisions of the active space that can be combined with different levels of excitations. Instead of a complete active space (CAS) where all possible distributions of the active electrons in the active orbitals are taken into account, a restricted active space (RAS) is employed where the active orbitals are further subdivided into three subspaces: RAS1, RAS2, and RAS3. The orbitals in RAS1 are doubly occupied apart from allowing a maximum number of holes, while in RAS3 the orbitals are empty apart from allowing a limited number of electrons. In RAS2, all remaining active electrons are distributed over the orbitals, like in the original CAS. This whole procedure makes the RASSCF/RASPT2 method much less systematic than CASSCF/CASPT2. The previous RASPT2 study[6] mainly focused on the electronic spectroscopy of organic molecules. Only two simple TM systems, $CuCl_4^{2-}$ and the Ni atom, were considered, giving particular attention to the description of the so-called 3d double-shell effect[11] by means of RASPT2 rather than CASPT2.

The present paper aims at providing a more systematic overview of the possibilities and limitations of the RASSCF/RASPT2 method in the field of (first-row) TM chemistry. The specific electronic structure of TM complexes, originating from a partially filled d shell surrounded by a number of potential electron-donating or -accepting ligands, gives rise to specific strong correlation effects which cannot be handled by second-order perturbation theory and should therefore be included already in the reference wave function (be it of CAS or RAS type). Two types of such strong correlation effects are by now

Received: August 24, 2011
Published: October 20, 2011

generally known and have become the basis for the 'standard' rules for contructing the active space for TM systems.[12−16]

- Nondynamic correlation effects connected to covalent TM−ligand interactions, giving rise to a set of bonding and antibonding molecular orbitals with mixed 3d−ligand character should be dealt with by including both combinations in the active space. Shortly, all valence molecular orbitals containing a significant metal d contribution should be active.
- The 3d double-shell effect. This correlation effect is important in systems with a high 3d occupation number, in particular if the d-orbital occupation changes between two states considered. It has to be dealt with in the reference wave function by including a second d shell, called either 3d′ or 4d, in the active space.

These two simple rules, however, are only the basis of an often much more complicated process of choosing active orbitals. For example, the first rule only suffices to describe the ground-state and metal-centered (MC, also called ligand field LF) excited states in complexes with weakly covalent bonds (for a counterexample, see the case of CrF_6 in Section 3.1). Moreover, it should always be kept in mind that the active space should not only include molecular orbitals involved in strong correlation effects but also orbitals that are or become partially occupied in the process studied. When describing, e.g., an electronic spectrum, the number of such orbitals may become quite large. The latter point is of course not specific to TM chemistry. However, in TM complexes the combination of covalency effects, double-shell effect, and the possible occurrence of different types of excited states [MC, charge-transfer (CT), either metal-to-ligand (MLCT) or ligand-to-metal (LMCT), and ligand-centered (LC)] may quite easily lead to a complex exercise of selecting active orbitals in a way that ensures a reasonable accuracy from the perturbation treatment, while keeping the size of the active space computationally manageable (i.e., up to about 16 orbitals in a CAS). The recent implementation of the RASPT2 method may have simplified this aspect of the calculational setup, as it allows for a less strict selection of the total number of active orbitals. However, the selection of the different subspaces and excitation levels (out of RAS1, into RAS3) within the RAS active space now becomes an additional crucial task that, in the case of TM complexes, has so far been virtually unexplored. How far can one go in moving orbitals involved in strong correlation effects, either due to covalent TM−ligand bonding or double-shell effects, from RAS2 into either RAS1 or RAS3, and which excitation level would then be required to maintain a similar accuracy in RASPT2 as compared to CASPT2? Should the orbitals that are involved in electronic excitations be included in RAS2 or not? Questions like this will be given an appropriate answer in the discussion below.

The aim of this contribution is to to design reliable strategies for general purpose RASPT2 calculations in TM chemistry. For that purpose, we have included a series of TM systems and chemical problems that should cover a broad range of typical correlation problems encountered when computing TM complexes. The systems chosen are chromium hexafluoride CrF_6, chromium hexacarbonyl $Cr(CO)_6$, ferrocene $Fe(Cp)_2$ (Cp = cyclopentadienyl), iron oxide FeO and its anion FeO^-, ferrous porphin Fe(P) (P = porphin), and cobalt corrole Co(C) (C = corrole). With exception of the last system, all of these molecules have been studied before by means of CASPT2, although with varying success.[14,17−23] The specific problems encountered for each molecule will be introduced in the appropriate section, and a detailed investigation of possible solutions coming from RASSCF/RASPT2 will be presented.

2. COMPUTATIONAL DETAILS

All CASSCF/CASPT2 and RASSCF/RASPT2 calculations were performed with the MOLCAS-7 program[24] making use of relativistic atomic natural orbital (ANO-rcc) type basis sets.[25,26] Unless noted otherwise, the contractions used are [7s6p5d3f2g1h] for the metal, [4s3p2d1f] on first-row atoms C, N, O, F, and [3s1p] on H. Scalar relativistic effects were included using a standard second-order Douglas−Kroll−Hess (DKH) Hamiltonian.[27−30] In all CASPT2/RASPT2 calculations, the core electrons, i.e., 1s from (C, N, O, F) and 1s−2p from the metal, were kept frozen. All CASPT2 and RASPT2 calculations in this work were performed using the standard ionization potential electron affinity (IPEA) Hamiltonian[31] (a zeroth-order Hamiltonian containing an IPEA shift = 0.25 au has become standard since MOLCAS-6.4). To avoid weak intruder states and improve convergence of the perturbational treatment, an imaginary level shift of 0.1 au was used.[32] Furthermore, in all calculations advantageous use (in terms of computational times and disk storage needs) was made of the Cholesky decomposition of the electron repulsion integral matrix[33−35] (with a threshold of $\delta = 10^{-6}$ au).

The specific choice of the actives spaces used to construct the CASSCF and RASSCF reference wave function is of course different for each of the considered molecule and will therefore be presented in the appropriate section of the results. However, it is important to describe here the notation employed to label the CASSCF and RASSCF active spaces. For the CASSCF calculations, the traditional notation will be used, i.e., CAS(n,a), where n is the number of electrons included in the active space and a is the number of active orbitals. For the RASSCF calculations, the short notation RAS(n,a) will be maintained to denoted the global active space. However, the RAS subpartitions and excitation levels are now specified by a longer notation, RAS(n,l,m;i,j,k) with l the maximum number of holes allowed in RAS1 and m the maximum number of electrons to enter RAS3. Active orbitals are labeled i,j,k (with $i + j + k = a$) and refer to those placed in RAS1, RAS2 and RAS3, respectively. Sometimes we will also use SD, SDT, SDTQ, etc., to denote the maximum excitation level out of RAS1 and/or into RAS3 (SD corresponding to $l = m = 2$, SDT to $l = m = 3$, ...).

In several cases, RASSCF calculations involving high excitation levels have been performed without performing an actual orbital optimization, i.e., they are in fact CI calculations based on orbitals obtained from a calculation with the same RAS but at a lower excitation level, usually SD. The primary motivation for considering this option is that RASSCF orbital optimizations, in the present version of the MOLCAS code, are really poorly convergent. Of course, such a procedure can only be successful if the effect of the higher excitations on the shape of the molecular orbitals is minimal. Extensive testing to prove this has been performed in case of CrF_6 (Section 3.1) and Co(C) (Section 3.5). Further specifications on the orbital optimization levels used will be given in each section.

Most calculations performed in this work are single-point calculations. Only for FeO/FeO^-, structures were optimized at the CASPT2/RASPT2 level. In all other calculations, structures were used that were taken either from experiment, from DFT

Table 1. Relative Energy (kcal/mol) of the Trigonal Prismatic and Octahedral Structure of CrF_6 at Different Computational Levels

	CASPT2(10,10)	RASPT2(42,*l*,*m*;21,0,5)			RASPT2(42,*l*,0;16,10,0)	
orbitals		SD	SDTQ	SDTQ56	SD	SDTQ
fully optimized	49.0	8.1	15.0		12.8	
taken from SD		8.1	15.4	16.5	12.8	17.8

structure optimizations, or from previously reported calculations. More precise details will be given in the appropriate sections.

3. RESULTS AND DISCUSSION

3.1. Relative Energies of the Octahedral and Trigonal Prismatic Structure of CrF_6. Considering correlation effects, the CrF_6 molecule does not exactly behave as a 'typical' TM complex. The extremely high formal oxidation state of chromium, +VI, gives rise to very strong covalency in the Cr−F bonding and correspondingly strong static correlation effects. Within octahedral symmetry, covalent-bond formation at the molecular orbital level is only possible within the representations e_g, t_{2g}. This type of covalency may adequately be described by a (10,10) active space, including the bonding and antibonding Cr 3d−F 2p combinations within these two representations. An early CASPT2 calculation along this line was performed to calculate the relative energies of the octahedral (O_h) and trigonal prismatic (D_{3h}) structure of CrF_6.[17] This calculation, however, turned out to strongly overestimate the stability of the octahedral with respect to the trigonal structure, predicting an energy difference of 49.9 kcal/mol, while corresponding values of 14.4 and 16.9 kcal/mol were obtained from coupled-cluster singles and doubles and perturbative triple excitations [CCSD(T)] and DFT(B3LYP), respectively.[36,37] The origin of the CASPT2 error was analyzed later[14] by means of a RASSCF calculation, including all F 2p orbitals in the active space, and was found to be due to the occurrence of large contributions in the ground-state wave function of excitations from the nonbonding F 2p orbitals into Cr 3d. A more accurate perturbational treatment would therefore have to start from a reference wave function including all such excitations, being built from an active space including 36 electrons in 23 (Cr 3d + F 2p) orbitals. Such a calculation is out of reach of CASPT2 but can quite easily be performed with RASPT2. In fact, the RASPT2 calculations presented here were performed with an even larger RAS(42,26) space, including also the Cr 3p shell, which was found to mix quite strongly with some of the F 2p orbitals. Two subdivisions of this global active space were considered: (A) RAS(42,*l*,*m*;21,0,5) ($l = m = 2,4,6$), i.e., with RAS2 empty, F 2p and Cr 3p in RAS1, and Cr 3d in RAS3; (B) (42,*l*,0;16,10,0) ($l = m = 2,4$) with RAS3 empty, and RAS2 now consisting of the bonding and antibonding Cr 3d−F 2p combinations providing the CAS(10,10) space in the original CASPT2 study.[17] The SDTQ calculations with active space A were performed either using fully optimized orbitals or using fixed orbitals taken from the corresponding SD calculation. For the SDTQ56 calculations with active space (A) and for SDTQ with active space B, only fixed orbitals were used. In order to compare the RASPT2 results with our previous CASPT2 calculations,[17] the present CASPT2 and RASPT2 calculations on CrF_6 were performed on O_h and D_{3h} structures taken from that work. The results are presented in Table 1.

The main point to be noted from Table 1 undoubtedly is the huge difference between the results obtained from either CASPT2 or RASPT2. Comparing CASPT2(10,10) with RASPT2-(42,2,0;16,10,0) we find that moving all F 2p−Cr 3d (and Cr 3p−3d) correlation effects from the perturbational treatment to the active space and treating them variationally with SD gives a lowering of the energy barrier by as much as 36 kcal/mol. The differences between the distinct RASPT2 treatments are much more limited. With RAS2 empty, the results obtained with only up-to-double RAS1 → RAS3 excitations are clearly too low. Up to sextuple excitations are necessary to provide a (more or less) converged RASPT2 result. Note that the two results obtained with SDTQ, making use of either orbitals obtained from the SD calculation or reoptimized, differ by less than 1 kcal/mol, thus indicating that orbital optimization at this level is not strictly necessary. After moving the bonding and antibonding Cr 3d−F 2p combinations to RAS2, significantly better results are obtained already at the SD level. Notably though, also in this case a further improvement by as much as 5 kcal/mol may be obtained by raising the excitation level to SDTQ. Unfortunately, the combination of a 10 orbital RAS2 with up to sextuple excitations is computationally unfeasible, such that it cannot be verified that the (42,4,0;16,10,0) is indeed (close to) converged. In any case, the two 'best' results obtained from RASPT2, 16.5 vs 17.8 kcal/mol, are rather close and also compare well to the earlier results obtained from DFT and CCSD(T), 14.2−16.9 kcal/mol.[36,37] In conclusion, these calculations on CrF_6 present a clear-cut (first) example of a multiconfigurational problem that was unsolvable before with CASPT2 because of limitations in the size of the CAS space and for which the extension to RAS provides a considerable and very valuable improvement of the multiconfigurational perturbation treatment.

3.2. Heterolytic Binding Energy of Ferrocene. One of the first CASPT2 studies in organometallic chemistry, by Pierloot, Persson, and Roos (PPR) in 1995,[19] concerned the equilibrium structure and binding energy of ferrocene. In particular, the heterolytic dissociation energy of the reaction $Fe(Cp)_2 \rightarrow Fe^{2+}(^5D) + 2Cp^-$ was an important test case for this method. An accurate description of this property can only be obtained when all important (nondynamic) correlation effects connected to the covalent bonding between the Fe^{2+} ion and the two cyclopentadienyl (Cp^-) ligands are adequately treated. Starting from an MP2 treatment, which was found to overestimate the binding energy by about 50 kcal/mol, a successful CASPT2 treatment was obtained by extending the reference wave function from Hartree−Fock to CASSCF with a (10,10) active space (specifications are given below). After correcting for basis set superposition errors (BSSE), the 'best' CASPT2 value for the heterolytic dissociation energy was 628 kcal/mol, in close

Table 2. ANO-rcc Basis Set Contractions Used for the CASPT2/RASPT2 Calculations on Ferrocene

atom	VTZP (I)	VQZP (II)	V8ZP/V5ZP (III)	V8ZP/V7ZP/V6ZP (IV)
Fe	6s5p3d2f1g	7s6p4d3f2g1h	10s9p8d6f4g2h	10s9p8d6f4g2h
C	4s3p2d1f	5s4p3d2f1g	6s5p3d2f1g	8s7p4d3f2g
H	3s2p1d	4s3p2d1f	5s3p2d1f	6s4p3d1f

Table 3. Basis set superposition errors (kcal/mol) obtained with CASPT2 and different basis sets

	basis I	basis II	basis III	basis IV
Without Fe (3s,3p) Correlation				
Fe^{2+} + 2 Cp(ghost)	4.8	2.4	0.1	0.1
Cp^- + Fe(ghost) + Cp(ghost)	9.7	3.7	3.1	1.1
sum	24.2	9.8	6.3	2.3
Including Fe (3s,3p) Correlation				
Fe^{2+} + 2 Cp(ghost)	30.9	21.7	0.6	0.9
Cp^- + Fe(ghost) + Cp(ghost)	9.7	3.7	3.1	1.1
sum	50.3	29.1	6.8	3.1

agreement with the value of (635 ± 6) kcal/mol reported from experiment[38] for the heterolytic bond disruption enthalpy of ferrocene. Admittedly, the close agreement with experiment was to some extent fortuitous, being the result of a cancellation of errors related to the (limited) size of the basis sets, the absence of zero-point vibrational energy (ZPVE) and thermal corrections and the rather crude treatments of relativistic effects and of Fe (3s,3p) (semicore) correlation. As a matter of fact, the (ANO-s) basis set used for iron in the PPR study[19] is not properly designed for treating (3s,3p) correlation,[39] giving rise to huge BSSE on Fe. Therefore, semicore correlation was in the PPR study only included for the calculation of the $^1I-{}^5D$ excitation energy in Fe^{2+} but was omitted for the dissociation step. A critical analysis of the different sources of errors in the CASPT2 treatment of ferrocene was presented in a later paper by Klopper and Lüthi,[40] who concluded that, when extrapolated to the basis set limit, the heterolytic bond disruption enthalpy of ferrocene obtained from CASPT2(10,10) would be ΔH^0_{298} = 657 kcal/mol, around 20 kcal/mol higher than the experimental value of (635 ± 6) kcal/mol. This would suggest that CASPT2, based on a CAS(10,10) reference wave function, inherently quite strongly overestimates the binding energy in this molecule. (Notably though, extrapolated to the basis set limit, the CASPT2 binding energy was very similar to the result obtained using coupled cluster theory.)[41]

In this work, the heterolytic binding energy of ferrocene is revisited by means of CASPT2 and RASPT2. Developments in the MOLCAS software over the last years have made it possible to strongly reduce the errors afflicting the reliability of the early CASPT2 results. In particular new ANO-rcc basis sets, constructed making use of the Douglas−Kroll Hamiltonian, should provide an accurate description of scalar relativistic effects.[25,26] For the TM, these basis sets were designed to treat semicore correlation, leading to more a accurate description of this type of correlation and smaller BSSE. Moreover, the latter errors may be circumvented by making use of much more extended contracted basis sets, thanks to the recent advent in MOLCAS of the Cholesky decomposition technique to approximate the two-electron integrals and its combination with CASPT2/RASPT2.[33−35] Four different combinations of ANO-rcc contraction schemes, denoted I−IV and shown in Table 2, were used in this section, the largest combination giving rise to 1457 contracted functions.

3.2.1. Computational Details. Ferrocene has a ground-state geometry where the two pentadienyl rings are eclipsed, with the staggered conformation approximately 1 kcal/mol higher in energy. The point group symmetry of the eclipsed structure is D_{5h}, and the calculations were performed within the highest abelian subgroup symmetry C_{2v}.

Single-point calculations on the experimental geometry of ferrocene[42] were performed, with the following distances: R(C−C) = 1.440 Å, R(C−H) = 1.104 Å, and R(Fe−Cp) = 1.66 Å. For free Cp^- a D_{5h} structure was optimized by means of MP2 making use of the smallest VTZP basis set (I), giving R(C−C) = 1.397 Å and R(C−H) = 1.079 Å. All binding energies reported include a correction for the BSSE, obtained by means of the full counterpoise method, i.e., from a calculation either on Fe^{2+} adding ghost orbitals of the two rings and on Cp^- adding ghost orbitals of Fe^{2+} plus the other ring. BSSE were calculated for all combinations of methods and basis sets. However, using the same basis sets the differences between the RASPT2 and CASPT2 results are insignificantly small (<1 kcal/mol). Therefore, only the CASPT2 results are given in Table 3. To be able to compare the calculated results for the binding energies to the experimental value of the heterolytic bond disruption enthalpy, ΔH^0_{298} = (635 ± 6) kcal/mol,[38] a correction for the difference in zero-point vibrational energy (−9.3 kcal/mol), and the thermal correction to the reaction enthalpy (13/2 RT + the difference in vibrational energies = 2.9 kcal/mol) were estimated from DFT optimizations and frequency analyses on ferrocene and Cp^-, making use of the BP86 functional and extended basis sets (def2-QZVPP on Fe, def2-TZVP for C,H). Rather than adding these corrections to all calculated CASPT2/RASPT2 binding energies, we have chosen to compare the uncorrected data to a 'corrected' experimental heterolytic binding energy of (641 ± 6) kcal/mol.

3.2.2. CASPT2 Calculations: Results and Discussion. First, a set of CASPT2 calculations was performed with different basis sets, making use of the same CAS(10,10) active space that was used in the PPR study.[19] This active space includes those pairs of orbitals that are directly involved in covalent Fe−Cp interactions: the (4,5)e''_1 shells, consisting of the bonding and antibonding combinations of Cpπ and the (formally empty) Fe (d_{xz},d_{yz}) orbitals, and the (4,5)e'_2 shells, incorporating the backdonation from the (formally doubly occupied) Fe (d_{xy},$d_{x^2-y^2}$) orbitals into the Cpπ^*orbitals of the same symmetry. We note though that the $5e'_2$ shell also contains significant Fe 3d′ character (for a more detailed analysis of the covalent interactions in ferrocene see ref 19). On top of this (8,8) space, the essentially nonbonding Fe $3d_{z^2}$ orbital of a'_1 symmetry and its correlating 3d′ orbital were also included. In the heterolytic dissociation limit, this active space is split into a CAS(6,8) space on Fe^{2+} (five 3d and three correlating 3d′ orbitals) and a CAS(4,2) space on Cp^-, the latter therefore being described by MP2 rather than CASPT2. However, since the dissociation proceeds to the Fe(II) ^5D ground

Table 4. Binding Energies[a] (E_b) for the Reaction $FeCp_2 \rightarrow Fe^{2+}(^5D) + 2Cp^-$ (kcal/mol)

	basis I	basis II	basis III	basis IV
Without Fe (3s,3p) Correlation				
CASPT2(10,10)	618.5	635.3	639.1	641.1
RASPT2(14,2,2;3,8,7)	605.1	622.4	625.5	627.1
Including Fe (3s,3p) Correlation				
CASPT2(10,10)	633.2	650.9	655.1	657.2
RASPT2(14,2,2;3,8,7)	619.1	637.2	640.5	641.4
RASPT2(14,4,4;3,8,7)	619.2			
RASPT2(14,6,6;3,8,7)	618.8			
RASPT2(14,2,2;7,0,11)	610.5	628.6	632.4	
RASPT2(14,4,4;7,0,11)	630.0	647.7	651.4	
RASPT2(14,6,6;7,0,11)	632.0			
RASPT2(14,8,8;7,0,11)	632.2			
expt		(641 ± 6)		

[a] Corrected for BSSE.

state with all 3d orbitals at least singly occupied, we chose to calculate the energy of the Fe^{2+} fragment using a full 3d′ shell in the active space of the fragment iron cation, i.e., CAS(6,10) rather than with the unbalanced CAS(6,8) space.

All calculated binding energies are presented in Table 4. At the CASPT2 level, calculations with and without Fe (3s,3p) correlation were performed, and the results in Table 4 clearly indicate that iron semicore correlation is important and should be included when calculating the binding energy, increasing the results with up to 16 kcal/mol. However, as indicated by Table 3, including the Fe(3s,3p) electrons in the correlation treatment drastically increases the BSSE on iron, at least with the smallest contractions (basis I, II). As the BSSE is very large, its (counterpoise) correction may not be very reliable. Therefore, we decided to extend the basis sets up to a point where the BSSE would become small enough, i.e., lower than the errors that might arise from the CASPT2/RASPT2 treatment. Comparing the results with different basis sets in Table 4, one can observe an important increase of the binding energy, about 22−24 kcal/mol, with the size of the basis sets. Making use of the largest basis set IV and including iron semicore correlation, the heterolytic binding energy of ferrocene obtained from CASPT2 amounts to 657.2 kcal/mol. This result is considerably larger than the binding energy from the original CASPT2 study (628 kcal/mol).[19] As compared to experiment, CASPT2 seems to overestimate the total strength of the Fe−Cp bonds by at least 10 kcal/mol. Given the extended size of the basis sets employed here, the source of the remaining error should be traced back to the CASPT2 method itself and more specifically to the limited size of the CAS(10,10) reference wave function.

3.2.3. RASPT2 Calculations: Results and Discussion. In order to investigate the effect of the active space on the binding energy, a second series of calculations was performed with a larger active space, however now making use of RASPT2 instead of CASPT2. The CAS(10,10) space was extended with the $6e_1'(Cp\pi)$, $3e_2''(Cp\pi^*)$ couple as well with the remaining four Fe 3d′ orbitals, thus giving RAS(14,18). As for CrF_6 in the previous section, two options for subdividing this active space were investigated, i.e., (A) with RAS2 comprising the $(4,5)e_1''$, $(4,5)e_2'$ shells involved in covalent Fe 3d−Cpπ interactions → RAS(14,*l*,*m*;3,8,7), and (B) with an empty RAS2 space → RAS(14,*l*,*m*;7,0,11). Upon dissociation, the global RAS(14,18) active space is split into a RAS(6,10) space on iron (all 3d, 3d′ orbitals) and a RAS(4,4) π space on Cp^- (while taking care of the appropriate subdivisions corresponding to (A) or (B) in $FeCp_2$). For the fragments, an excitation level $l = m = 2$ was used in all calculations. In order to obtain a fully size-extensive treatment, this means that up to sextuple excitations should be allowed for $FeCp_2$. In order to check this, test calculations with $l = m = 4,6$ were performed with the smallest basis sets (making use of full CI calculations with the orbitals taken from the SD calculation).

We first consider the RASPT2 calculations performed with the RAS(14,2,2;3,8,7) space. Such calculations were performed with all four basis sets and both with and without semicore correlation. As can be seen from Table 4, the effect of Fe (3s,3p) correlation on the binding energy is similar for the RASPT2 and CASPT2 calculations, giving rise to a bond strengthening by about 15 kcal/mol. Both with and without (3s,3p) correlation, the RASPT2-(14,2,2;3,8,7) binding energy is systematically lower than the CASPT2 binding energy by 13 kcal/mol, a value which does not significantly depend on the size of the basis set. We also note the very small differences between the results obtained at different excitation levels *l*, *m* = 2−6. When keeping in RAS2 the eight orbitals that are responsible for the most important nondynamic correlation effects, $(4,5)e_1''$, $(4,5)e_2'$, the RASPT2 treatment of $FeCp_2$ converges already at the SD level. However, it is clear that the variational treatment in the RASSCF wave function of extra important correlation, i.e., the full Fe 3d double-shell effect and the most important Cp^- $\pi-\pi^*$ correlation effects, has a substantial effect on the result of the perturbational treatment, lowering the binding energy by more than 10 kcal/mol. With the largest basis set IV and including semicore correlation, the heterolytic dissociation energy of $FeCp_2$ obtained from RASPT2 amounts to 641.1 kcal/mol, as compared to the experimental value of (641 ± 6) kcal/mol.

Less satisfactory results are obtained from the RASPT2 calculations with an empty RAS2 space. As Table 4 shows, the binding energies obtained from the RASPT2(14,2,2;7,0,11) calculations are considerably lower, by 8−9 kcal/mol, than the corresponding results with RASPT2(14,2,2;3,8,7). On the other hand, between SD and SDTQ the binding energies from the empty RAS2 calculations are increased by 19−22 kcal/mol, while the calculations with the eight-orbital RAS2 are already converged at the SD excitation level. With an empty RAS2, convergence is reached only with SDTQ rather than with SD. However, the ultimate binding energy, 651.4 kcal/mol (with basis III, a slightly higher value may be anticipated for basis IV) is now higher by 11 kcal/mol than the result obtained from the eight-orbital RAS2 calculation.

The question may of course be raised as to why the two sets of RASPT2 calculations presented in Table 4 converge to such strongly different values of the binding energy. Should they not both converge to the same full CI limit, being then also the answer that would be obtained from a full CASPT2(14,18) calculation? That this is not the case is related to the way a RASPT2 calculation is designed in its current implementation in the MOLCAS code. As with CASPT2, a RASPT2 calculation starts with the construction of an effective Fock matrix. In the CASPT2 case, this Fock matrix is diagonalized within the three subspaces inactive/inactive, active/active, and external/external. Note that unitary transformations of the orbitals within these three subspaces do not affect the overall CASSCF wave function.

Table 5. Relative Energies of the Most Important LF and CT Excited States in $Cr(CO)_6$

method	$^1T_{1g}$	$^1T_{2g}$	a^1T_{2u}	a^1T_{1u}	b^1T_{2u}	b^1T_{1u}
CASPT2(10,16)	4.92	5.35	3.88	4.31(0.20)	4.68	5.16(2.44)
MS-CASPT2(10,16)	4.92	5.35	3.87	4.29(0.42)	4.69	5.18(2.18)
RASPT2(10,3,3;5,0,11)[a]	4.50	4.94	3.47	3.89(0.22)	4.26	4.91(2.55)
RASPT2(10,3,3;5,0,11)[b]	4.65	5.09	3.62	4.03(0.22)	4.41	5.06(2.54)
RASPT2(10,5,5;5,0,11)[c]	4.86	5.28	3.69	4.11(0.22)	4.47	5.10(2.53)
RASPT2(10,5,5;5,0,11)[d]	4.88	5.31	3.71	4.14(0.22)	4.50	5.12(2.54)
RASPT2(10,7,7;5,0,11)[e]	4.92	5.35	3.74	4.16(0.22)	4.61	5.14(2.54)
RASPT2(10,0,2;0,10,6)	4.92	5.35	4.06	4.50(0.17)	4.89	5.43(2.37)
RASPT2(10,0,3;0,10,6)	4.92	5.35	3.87	4.30(0.20)	4.67	5.14(2.47)
RASPT2(10,0,4;0,10,6)	4.92	5.35	3.86	4.29(0.20)	4.67	5.14(2.43)
RASPT2(10,0,2;0,10,14)	4.75	5.08	3.96	4.40(0.20)	4.83	5.27(2.56)
RASPT2(10,0,3;0,10,14)	4.98	5.23	4.07	4.50(0.20)	4.91	5.43(2.61)
RASPT2(10,0,4;0,10,14)	4.98	5.23	4.07	4.50(0.20)	4.91	5.42(2.57)
MS-RASPT2(10,0,4;0,10,14)	4.98	5.23	4.06	4.47(0.46)	4.91	5.45(2.26)
expt[f]				4.44(0.25)		5.48(2.3)

[a] Using SD for GS. [b] Using SDT for GS. [c] Using SDTQ for GS. [d] Using SDTQ5 for GS. [e] Using either SDTQ56 or SDTQ567 for GS. [f] From Beach and Gray.[43]

Within the basis of the resulting 'canonical' orbitals, all off-diagonal Fock matrix elements connecting active orbitals are zero. This is, however, not the case in RASPT2. Here, orbital rotations that couple different RAS subspaces, i.e., RAS1 and RAS2, RAS1 and RAS3, and RAS2 and RAS3, are not allowed. Thus, the diagonalization of the active part of the Fock matrix is not complete in RASPT2, as it is in CASPT2, but instead nonzero elements may remain in the parts that couple different RAS subspaces. In the current implementation of RASPT2 these elements are ignored, and the coupling is thus not accounted for in the perturbation. If the coupling elements are large, then this may lead to RASPT2 results that are strongly different from the corresponding CASPT2 solution or from an alternative RASPT2 solution which does include the strongly interacting orbitals in the same RAS subspace. This is the case here, with the bonding−antibonding Fe 3d−Cpπ combinations allowed to rotate among each other in the calculations with the (4,5)e_1'', (4,5)e_2'' couples in RAS2, but not in the empty RAS2 calculations, the former calculation obviously giving superior RASPT2 results. The present example indicates that, in order to provide an accurate description of the metal−ligand binding in covalently bonded TM complexes by means of RASPT2, the orbitals involved in the covalent interaction should preferably be kept together in RAS2.

3.3. Electronic Absorption Spectrum of $Cr(CO)_6$. The UV gas phase absorption spectrum of $Cr(CO)_6$ has been intensively studied in the past, both experimentally and theoretically, and its assignment is by now well established. The experimental spectrum with its assignment was first reported in 1968.[43] Two intense bands at relative energies of 4.44 and 5.48 eV were assigned as symmetry allowed $^1A_{1g} \rightarrow {}^1T_{1u}$ MLCT transitions, whereas two weak features at the red tail of the spectrum were originally assigned as ligand-field (LF) excitations. The latter assignment was, however, revised in the first CASPT2 study of the spectrum,[20] which indicated that the two singlet LF states, $^1T_{1g}$ and $^1T_{2g}$, should in fact be situated at much higher energies than originally proposed and that the absorption features at the red tail of the spectrum are rather due to orbitally forbidden MLCT excitations. The latter assignment was soon confirmed in a ΔSCF-DFT study by Pollak et al.,[44] who also proposed a reassessment of the role of the LF states in the photochemistry of $Cr(CO)_6$ and other metal−carbonyl complexes. Starting from then, the electronic spectra of $Cr(CO)_6$ and other metal carbonyl complexes $M(CO)_6$ (M = Cr, Mn^+, V^-, Mo, W) have frequently been used in benchmarking studies by means of time-dependent DFT (with different functionals),[45,46] DFT/multireference configuration interaction (DFT/MRCI),[47] CASPT2,[48] and coupled-cluster methods.[48,49]

$Cr(CO)_6$ is an octahedral molecule with a closed-shell $^1A_{1g}$ ground state corresponding to the configuration $2t_{2g}^6 6e_g^0$. The bonding in this molecule is built from two interactions with quite strong covalent character: σ-donation from CO into the formally empty $6e_g$(Cr 3d) orbitals, counteracted by π backdonation from the fully occupied $2t_{2g}$(Cr 3d) orbitals into the COπ^* orbitals of the same symmetry. In order to describe the nondynamic correlation effects connected to these covalent interactions, a CAS(10,10) active space, including the Cr 3d orbitals and their bonding $5e_g$ and antibonding $3t_{2g}$ counterparts, is necessary. However, this CAS(10,10) space is not appropriate to describe the two most intense bands in the electronic spectrum, of $^1T_{1u}$ symmetry, corresponding to charge-transfer excitations into the $9t_{1u}$ and $2t_{2u}$ COπ^* shells. To describe these states, the 'basic' CAS(10,10) space has to be extended with both these shells, giving a CAS(10,16) space. At the time of our original CASPT2 study of the $Cr(CO)_6$ spectrum, an active space of this size was computationally out of reach. This is no longer the case now, and in this work, we will start from a CASPT2(10,16) calculation of the most important bands in the $Cr(CO)_6$ spectrum. Starting from this CASPT2(10,16) calculation, several RAS spaces are then construced, serving two goals: (A) to explore the adequacy of RASPT2 with the same global RAS(10,16) space but with different RAS partitions/excitation levels and (B) to extend the (10,16) active space with extra orbitals, finding ways to improve the accuracy of the calculations by comparing the results obtained for the excitation energies (oscillator strengths) of the two $^1T_{1u}$ states to the experimental data: 4.44 eV (0.25) and 5.48 eV (2.3). We will focus on just six excited states in the vertical spectrum of $Cr(CO)_6$, namely the two singlet LF states $^1T_{1g}$ and

$^1T_{2g}$, both corresponding to a $2t_{2g} \rightarrow 6e_g$ excitation, and four MLCT states a,b$^1T_{1u}$ and a,b$^1T_{2u}$, corresponding to excitations out of $2t_{2g}$ into either $9t_{1u}$ or $2t_{2u}$. All calculations were performed within D_{2h} symmetry but with extra restrictions to prevent mixing of orbitals belonging to different representations within O_h. State-average calculations were performed for the two LF excited states $^1T_{(1,2)g}$ and for the four MLCT states a, b$^1T_{(1,2)u}$, since these sets of states belong to the same symmetry species within D_{2h}. The calculations were performed for the experimental octahedral structure of $Cr(CO)_6$ with a Cr−C bond distance of 1.914 Å and a C−O distance of 1.140 Å.[50] The results are collected in Table 5.

The first two lines in Table 5 contain the CASPT2 data for the excitation energies and oscillator strengths obtained starting from the CAS(10,16) reference space. Both single-state and multistate (MS-CASPT2) results are given, the latter allowing for remixing of the wave functions of the pairs of $^1T_{1u}$ and $^1T_{2u}$ states under the influence of dynamical correlation (i.e., the CASPT2 treatment).[51] One can see that the energetic effect of the MS algorithm is very limited, whereas its effect on the relative oscillator strength of both allowed ($^1T_{1u}$) CT transitions is more significant. In fact, in absolute terms both pairs of oscillator strengths quite closely agree with experiment (the last line in Table 5). At the single-state level, the relative intensity of the second with respect to the first $^1T_{1u}$ state is slightly too high (12.2 versus 9.2 experimentally), whereas the MS treatment overcorrects, leading to a too small ratio (5.2). A detailed overview of the calculated excitation energies and corresponding spectral intensities at different computational levels for the two main bands in the UV absorption spectrum of $Cr(CO)_6$ was reported very recently.[47] We note that the values of the oscillator strengths obtained from the present CASPT2(10,16) calculations are, together with the DFT/MRCI results from ref 47 (0.234 for a$^1T_{1u}$, 2.203 for b$^1T_{1u}$), superior to any of the previously calculated values for this property. The same is, however, not the case for the CASPT2(10,16) excitation energies. As Table 5 indicates, the calculated excitation energies are too low, with the largest error, 0.30−0.32 eV, for the b$^1T_{1u}$ state. Even though the present and previous CASPT2 calculations show an accuracy which is good enough to provide a qualitative correct assigment of the $Cr(CO)_6$ UV absorption spectrum, there is obvious room for improvement, coming from RASPT2 calculations with an extended active space.

Before moving to these calculations it is, however, necessary to test the accuracy that can be obtained with different RAS(10,16) subpartitions/excitation levels with respect to the full CASPT2-(10,16) results. In Table 5 two different RAS(10,16) subpartions have been considered. In the first case, RAS2 is empty, and the different states in the spectrum are described by RAS1→ RAS3 excitations, starting from the closed-shell HF wave function of the ground state and allowing different maximum excitation levels. Since a single RAS1 → RAS3 excitation is involved already in the primary configuration of all excited states, the excitation levels given in Table 5 are uneven, i.e., an even number (doubles, quadruples, ...) to describe correlation on top of the single excitation creating the open shell. When comparing the energy of the excited states to the energy of the closed-shell ground state, it is not obvious a priori whether the same or one lower excitation level should be used for the latter state. Results of both approaches have therefore been included in Table 5. Their difference reflects the effect of the additional excitation on the ground-state correlation treatment and disappears as the latter treatment converges. As the results indicate, these RASPT2 calculations suffer from the same problems as noted already for the calculations with empty RAS2 for ferrocene, i.e., (a) slow convergence of the relative energies with the excitation level, and (b) the convergence limit (both for the excitation energies and oscillator strengths) does not equal the CASPT2 result, at least not for the CT excitations. The origin of these failures has been analyzed in detail in the previous section (Section 3.2). As for ferrocene, considerably better results may be obtained by including in RAS2 the 10 orbitals involved in the covalent Cr−CO interactions, leaving RAS1 empty and including only the t_{1u} and t_{2u} shells in RAS3. As can be seen from Table 5, the RASPT2(10,0,*m*;0,10,6) results are converged already at the SD excitation level for the LF states (adding triples cannot affect the energy of these gerade states as all RAS2 → RAS3 excitations are g → u) and at the SDT level for the CT states, with excitation energies and oscillator strengths that are virtually equal to the corresponding CASPT2(10,16) results. As a general rule, we would therefore like to state again that, in order to obtain accurate RASPT2 results for relative energies in (first-row) TM systems, all ligand orbitals involved in covalent metal−ligand interactions should be kept together with the metal 3d orbitals in the RAS2 space.

Starting from the second set of RASPT2 calculations, the global active space can now straightforwardly be extended with additional RAS3 orbitals that might be expected to play an important role in the correlation treatment, i.e., (a) an extra 3d′ shell (t_{2g}, e_g) providing an improved description of the 3d double-shell effect, and (b) the remaining CO π^* orbitals of t_{1g} symmetry. RASPT2 results obtained with this RAS(10,0, *m*;0,10,14) space are shown in the last block in Table 5. One can see that up-to-triple RAS2 → RAS3 excitations are now necessary to reach convergence for both the LF and CT states. At the SDT or SDTQ level, the RASPT2 results obtained with this 24-orbital active space are, however, significantly different from the corresponding 16-orbital results. This is particularly true for the four CT states, which are blue-shifted by 0.2−0.3 eV. The calculated excitation energies of the two allowed $^1T_{1u}$ states now approach their experimental band positions to within 0.06 eV; after allowing remixing in a MS treatment, the difference is further decreased to 0.03 eV. The effect of extending the active space on the calculated oscillator strengths is hardly significant. On the whole, the present calculations clearly illustrate the added value of RASPT2 with respect to CASPT2 for the accurate description of the electronic spectra of organometallic systems.

3.4. Spin-State Energetics in Ferrous Porphyrin. Because of the important role played by iron porphyrins in biological processes (as the active centers or prosthetic groups of hemeproteins), the electronic structure of the Fe(II) ion in ferrous porphyrins has since long been the subject of experimental and theoretical investigations. The most important experimental data were collected already many years years ago, between 1972 and 1985.[52−60] On the other hand, computational chemists became interested in the problem since the beginning of the 1980s and by now a large number of computational studies have been reported.[14,21,61−73] With six 3d electrons, the ground-state spin multiplicity of Fe(II) complexes may be either low-, intermediate-, or high-spin (S = 0, 1, or 2, respectively). In Fe(II) porphyrins, all three spin states may occur, depending on the coordination number and the environment of the iron ion. Experimental data[52−54] for the four-coordinate ferrous porphyrins tetraphenylporphinatoiron(II) (FeTPP)[52] and octaethylporphinatoiron(II) (FeOEP)[54,55] pointed to a triplet ground state

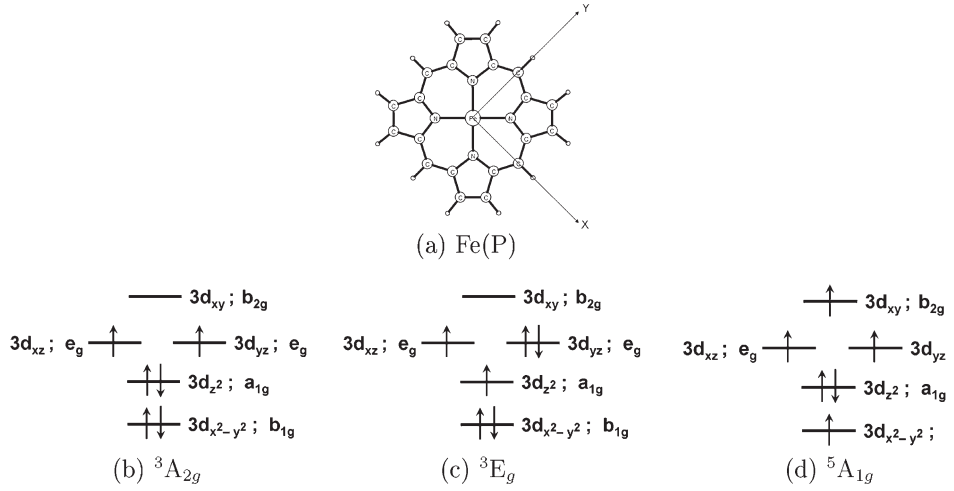

Figure 1. (a) Molecular structure of Fe(P), (b−d) orbital occupancy in the $^3A_{2g}$, ^3E_g(A), and $^5A_{1g}$ states.

but disagree on the details of the electronic configuration. For FeTPP, a $^3A_{2g}$ ground state was indicated by Mössbauer,[52,56] magnetic,[57] or proton nuclear magnetic resonance measurements.[53,58] On the other hand, resonance Raman spectra of FeOEP were originally interpreted in terms of a ^3E_g ground state.[54] The magnetic moments measured for these two complexes, 4.4 μ_B for FeTPP, and 4.6−4.7 μ_B for FeOEP,[55,59] are considerably higher than the pure triplet spin value 2.83 μ_B. This has been explained by the occurrence of one[53,56,58] or two[57] low-lying triplet states (^3E_g, $^3B_{2g}$) mixing through spin−orbit coupling (SOC) with the $^3A_{2g}$ ground state.

Obtaining accurate predictions of the spin state energetics in ferrous porphyrins has been shown in the past to be a real challenge for multiconfigurational perturbation theory (and other wave function methods). So far, all attempts to describe the relative energy of the low-lying states in free Fe(II) porphin (denoted as Fe(P) in what follows) have invariably predicted a high-spin ground state $^5A_{1g}$. A first attempt by means of multireference Møller−Plesset perturbation theory[65] found the $^5A_{1g}$ at 0.37 eV below the lowest triplet state, ^3E_g. In a subsequent CASPT2 calculation, the lowest triplet state was found to be $^3A_{2g}$, with ^3E_g at 0.02 eV. However, the $^5A_{1g}$ state was now even further stabilized with respect to the lowest triplet states, lying as much as 0.83 eV below $^3A_{2g}$. In 2003, it was shown by Pierloot[14] that the CASPT2 description of the relative spin state energetics may be considerably improved by an adequate choice of the active space, i.e., by including next to the Fe 3d orbitals, a set of five 3d′ orbitals to describe the 3d double-shell effect as well as one Fe−N σ bonding orbital to account for nondynamic correlation effects associated with the covalent-bonding character of the Fe 3d−$N_{(P)}$ σ bonds. With this CAS(8,11) space, the $^3A_{2g}$−$^5A_{1g}$ splitting was reduced to 0.44 eV. In the same article, it was also shown that including eight porphin π orbitals (the four highest occupied and four lowest unoccupied) in the active space does not affect the spin state energetics to any significant extent. More recently, the unbalanced description of the intermediate- and high-spin states in Fe(P) could be partially traced back to the formulation of the zeroth-order Hamiltonian $\hat{H}^{(0)}$ in the original formulation of CASPT2, which would systematically favor high-spin over low-spin states. In 2004 the alternative IPEA modified $\hat{H}^{(0)}$ was proposed and implemented as the standard (IPEA shift of 0.25 au) in MOLCAS.[31] Making use of the improved $\hat{H}^{(0)}$ and more extended basis sets, still using the same CAS(8,11) space as before, the CASPT2 $^3A_{2g}$−$^5A_{1g}$ splitting was further reduced to 0.19 eV (0.28 eV after correcting for the difference in zero-point vibrational energy).[21] A similar error was also found for the splitting between the lowest triplet and quintet state in small heme model systems (for which CCSD(T) results could be used as a benchmark) and in the five-coordinated Fe(P)(Im) complex (Im = imidazole).[22] From this it was concluded that the CASPT2 method has a systematic error of around 0.2 eV in favor of the high-spin state for ferrous heme complexes. Obviously, this error can only be explained by either the limited size of the active space or by limitations in the basis sets. Both options are explored in this work.

3.4.1. Computational Details. The basis sets used in the most recent CASPT2 calculations on Fe(P)[21] already consisted of quite extended ANO-rcc type sets. However, they did not provide a fully balanced treatment of the porphin ring, in that a larger contracted [4s3p2d1f] set on N was combined with a smaller [4s3p1d] set on C. In this work, the contracted basis set on C is also enlarged to [4s3p2d1f]. Other than that, the basis sets used in this work (ANO-rcc contracted to [7s6p5d3f2g1h] for Fe, [4s3p2d1f] for N, C, and [3s1p] for H) are the same as in ref 21.

CASPT2/RASPT2 calculations were performed for 11 low-lying states in Fe(P), with varying occupations of the Fe 3d orbitals and with different spins (S = 0−2). The orientation of the molecule in the xy-plane as well as the symmetry (in D_{4h}) and occupations numbers of the Fe 3d orbitals in the three lowest-lying states are shown in Figure 1. All calculations were performed at structures obtained from DFT, making use of the PBE0 functional and extended basis sets (def2-QZVPP on Fe, and def2-TZVPP on other atoms) and employing the Turbomole code.[74,75] Geometry optimizations were performed within D_{4h} symmetry, except for the ^3E_g(A) and ^5E_g states, for which D_{2h} symmetry was used (pointing to a very weak Jahn−Teller distortion). Individual DFT structures could be obtained for all states reported in Table 6, except for the second ^3E_g(B) state, the ^1E_g state, and the two open-shell singlet states $^1A_{1g}$(A) and $^1A_{2g}$. The CASPT2/RASPT2 calculations for the ^3E_g(B) and ^1E_g states were performed using the structure of the lower-lying ^3E_g(A) state, whereas for the open-shell singlets the structure of the $^3A_{2g}$ state (belonging to the same configuration) was used.

Table 6. Adiabatic Relative Energies (eV) of the Low-Lying Electronic States of Fe(P)

state	electronic configuration	CASPT2 (8,11)	RASPT2 (8,0,2;0,6,5)	RASPT2 (34,2,2;13,6,16)	CASPT2 (16,15)	RASPT2 (16,2,0;4,11,0)
$^3A_{2g}$	$(d_{x^2-y^2})^2(d_{z^2})^2(d_{xz},d_{yz})^2(d_{xy})^0$	0.00	0.00	0.00	0.00	0.00
$^5A_{1g}$	$(d_{x^2-y^2})^1(d_{z^2})^2(d_{xz},d_{yz})^2(d_{xy})^1$	−0.09	−0.19	−0.20	0.04	0.05
^3E_g(A)	$(d_{x^2-y^2})^2(d_{z^2})^1(d_{xz},d_{yz})^3(d_{xy})^0$	0.09	0.08	0.09	0.10	0.10
^3E_g(B)	$(d_{x^2-y^2})^1(d_{z^2})^2(d_{xz},d_{yz})^3(d_{xy})^0$	0.87	0.86	0.91	0.92	0.92
^5E_g	$(d_{x^2-y^2})^1(d_{z^2})^1(d_{xz},d_{yz})^3(d_{xy})^1$	0.12	0.01	−0.01	0.21	0.21
$^5B_{1g}$	$(d_{x^2-y^2})^2(d_{z^2})^1(d_{xz},d_{yz})^2(d_{xy})^1$	0.31	0.20	0.16	0.45	0.46
$^3B_{1g}$	$(d_{x^2-y^2})^1(d_{z^2})^1(d_{xz},d_{yz})^4(d_{xy})^0$	0.41	0.39	0.43	0.48	0.49
$^1A_{1g}$(A)	$(d_{x^2-y^2})^2(d_{z^2})^2(d_{xz},d_{yz})^2(d_{xy})^0$	1.29	1.30	1.30	1.30	1.24
$^1A_{2g}$	$(d_{x^2-y^2})^2(d_{z^2})^2(d_{xz},d_{yz})^2(d_{xy})^0$	1.31	1.31	1.31	1.30	1.29
^1E_g	$(d_{x^2-y^2})^2(d_{z^2})^1(d_{xz},d_{yz})^3(d_{xy})^0$	1.34	1.31	1.33	1.34	1.34
$^1A_{1g}$(B)	$(d_{x^2-y^2})^2(d_{z^2})^0(d_{xz},d_{yz})^4(d_{xy})^0$	1.52	1.47	1.52	1.64	1.64

3.4.2. Results and Discussion. The results of the CASPT2/RASPT2 calculations performed in this work are presented in Table 6. All reported energies are relative to the $^3A_{2g}$ state, which was found to be the lowest triplet at all calculational levels, with the lowest ^3E_g(A) state a 0.08−0.09 eV.

First, a set of CASPT2 calculations was performed based on the CAS(8,11) space described above. As expected, these calculations predict a high-spin, $^5A_{1g}$ ground state (with orbital occupancies shown in Figure 1c). Somewhat surprisingly, however, the $^3A_{2g}$ state is calculated at 0.09 eV, as compared to 0.19 eV in our (latest) previous CASPT2 study.[21] The difference between these two sets of results is due exclusively to the larger basis sets used in the present calculation.

Next, the CASPT2 calculations based on the CAS(8,11) space were confronted with a set of RASPT2 calculations making use of the same global active space RAS(8,11), however with the five Fe 3d′ orbitals placed in RAS3. With the excitation level limited to SD, this active space is noted as (8,0,2;0,6,5). From our previous RASPT2 benchmark study,[6] we have learned that the 3d double-shell effect may be reasonably well described (i.e., to within 0.1−0.2 eV as compared to the full CASPT2) with the correlating 3d′ shell moved from RAS2 to RAS3 and allowing only SD excitations. This finding is confirmed by the present results. Table 6 shows that moving the Fe 3d′ shell from RAS2 to RAS3 does not significantly affect the results obtained for the triplet and open-shell singlet states. The closed-shell $^1A_{1g}$(B) state is calculated 0.05 eV lower with RASPT2 than with CASPT2. However, a larger difference, 0.10 eV, is found for the quintet states. This difference is in line with previous results found for the Ni atom and copper tetrachloride,[6] where differences of 0.1 eV between CASPT2 and RASPT2 were generally considered acceptable. However, in the present case the consequence is a further increase of the error on the $^5A_{1g}$−$^3A_{2g}$ splitting at the RASPT2 level.

By putting the 3d′ shell in RAS3 we can, however, extend the global size of the RAS space to RAS(34,35), i.e., RAS(8,11) supplemented with the full set of 24 porphin π orbitals, containing 26 electrons. The 13 doubly occupied porphin π orbitals were put in RAS1, whereas the 11 π^* were added to the Fe 3d′ orbitals in RAS3. The results of this set of RASPT2(34,2,2;13,6,16) calculations are compared to the corresponding RASPT2(8,0,2;0,6,5) results in Table 6. Obviously, including the porphin π system in the active space does not significantly alter the relative energy of the different Fe 3d^6 states in this ferrous porphin. The three lowest-lying states are hardly affected, whereas for the higher states, differences of at most 0.05 eV are found between the two sets of results.

As a next option, we decided to run a set of CASPT2 calculations based on an active space of 15 orbitals and including 16 electrons, i.e., the CAS(8,11) space was extended with the Fe semicore (3s,3p) orbitals. It has been known for a long time[76] that intershell correlation effects between the 3d and the (3s,3p) shells may have a considerable effect on the relative energy of different low-lying states in first-row TM ions and their complexes. However, even if the first study of this effect already indicated that the CASPT2 results for the relative energies of different d^n states in TM ions are systematically (slightly) improved when including the semicore shells in the active space, this type of correlation has since then almost invariably been treated at the CASPT2 rather than at the CASSCF level. An obvious reason for this is that making four more orbitals active on top of all other, more important, valence and 3d′ orbitals would in many cases result in an active space which is too large to be handled by CASSCF/CASPT2. This is not the case here. Due to the high symmetry of Fe(P), CASPT2(16,15) calculations are perfectly possible. Furthermore, we can make use of this opportunity to test whether the (3s,3p)−3d intershell correlation effects may also be treated accurately by means of RASPT2 rather than CASPT2, i.e., by including the (3s,3p) shells in RAS1 and allowing up-to-doubles into the 3d shell. Relative energies obtained from both sets of calculations, CASPT2(16,15) and RASPT2(16,2,0;4,11,0), are given in Table 6. With exception of one state ($^1A_{1g}$(A), showing a difference of 0.06 eV), the two sets of results are close to within 0.01 eV, thus confirming that the semicore (3s,3p) orbitals may conveniently be placed in RAS1 rather than in RAS2. Treating the intershell correlation effects between the 3d and the (3s,3p) shells variationally by SD does, however, significantly affect the calculated relative energies of a number of specific states with respect to the $^3A_{2g}$ state, i.e., all quintet states and the closed-shell $^1A_{1g}$(B) state. As compared to CASPT2(8,11), the energy of the three quintet states is increased by 0.09−0.13 eV in the CASPT2(16,15) treatment, whereas the $^1A_{1g}$(B) state is shifted upward by 0.12 eV. The triplet and the open-shell singlet states are much less affected. As an important consequence, the $^3A_{2g}$ state is now predicted as the ground state of Fe(P), with both $^5A_{1g}$ and ^3E_g(A) low-lying, within 0.1 eV.

The data presented in Table 6 are adiabatic, i.e., they refer to CASPT2/RASPT2 energies obtained for optimized structures (with DFT) for each separate state. These structures are quite different, in particular the Fe−N distances, for the intermediate-spin

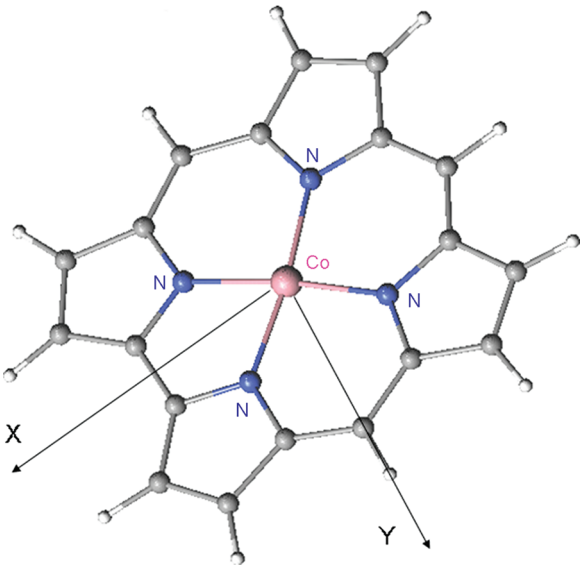

Figure 2. Molecular structure of cobalt corrole.

states $^3A_{2g}$, ^3E_g (R(Fe−N) = 1.989 Å for both states) and the high-spin state $^5A_{1g}$ (R(Fe−N) = 2.053 Å). When calculating instead the vertical electronic spectrum at the $^3A_{2g}$ and $^5A_{1g}$ structures, respectively, the $^5A_{1g}$ is only slightly raised at the $^3A_{2g}$ structure, to 0.08 eV, but it becomes the ground state at its own optimal structure, with both triplet states considerably raised in energy, lying at 0.32 eV ($^3A_{2g}$) and 0.40 eV (^3E_g) (with a second quintet state, ^5E_g, at 0.17 eV). With three close-lying states at the $^3A_{2g}$ structure (but not at the $^5A_{1g}$ structure), SOC may become important enough to significantly influence the relative energy between both structures. Moreover, mixing between the three states under SOC may be responsible for the high ground-state magnetic moment, 4.4−4.7 μ_B, observed experimentally for FeTPP and FeOEP.[55,59] Both premises were explored by treating SOC within the manifold of the seven lowest LF states (all states below 1.0 eV in Table 6), by means of the RAS state interaction (RASSI)-SOC method[29,77] making use of atomic mean-field integrals (AMFI).[78−80] The ground-state magnetic moment was calculated making use of the method presented in ref 81. The results of the calculations including SOC are presented in the Supporting Information. At the $^3A_{2g}$ structure, the ground state after SOC becomes a mixture of $^3A_{2g}$ (68%), ^3E_g (13%), and $^5A_{1g}$ (18%). The calculated magnetic moment is 4.43 μ_B, in close correspondence with the experimental values of 4.4−4.7 μ_B. This gives further support to the accuracy of the CASPT2(16,15) results for the relative energies of the three low-lying states in Fe(P). At the $^5A_{1g}$ structure the SOC wave function is found to be predominantly quintet: $^5A_{1g}$ (91%) and ^5E_g (5%), with a small (3%) $^3A_{2g}$ contribution. A magnetic moment of 5.57 μ_B is calculated for this state, slightly higher than the value for a pure quintet spin, 4.9 μ_B, due to the orbital contribution of the ^5E_g state. After SOC, the energy of the $^3A_{2g}$ structure is stabilized by 0.06 eV, the $^5A_{1g}$ structure by only 0.02 eV. As such, our 'best' estimate for the relative energy of both structures becomes 0.08 eV!

3.5. Low-Lying States of Cobalt Corrole. Corrole is a porphyrinoid compound in which one of the meso carbon atoms has been removed and replaced by a direct pyrrole−pyrrole bond. The remaining three meso positions remain occupied by carbon atoms. When fully deprotonated, corrolate becomes a trianionic ligand. The smaller trianionic corrolate ligand has a greater ability to stabilize higher central metal oxidation states than the larger dianionic porphyrinato ligand. On the other hand, the corrolate ligand is also easily oxidizable and may transfer one of its electrons to the central metal, e.g., in nickel and copper corrole,[9,82,83] to become itself 'noninnocent', i.e., a dianion radical. These special properties of corrolate have driven an intense investigation of TM corrole complexes.

Many experimental and theoretical studies have contributed to the characterization of cobalt corrole systems.[84−92] Based on the magnetic moment (3.2 μ_B) and ^{1}H NMR spectra (showing strong paramagnetic shifts) the Co(OEC) (OEC = octaethylcorrole) system was characterized as an intermediate-spin Co(III)(S = 1) center coordinated by a corrolate^{3-} ligand in a square planar coordination environment.[84] The corrole was in this system clearly indicated as an innocent ligand. As such, the cobalt(d^6) atom in Co-corrole is isoelectronic with the iron(d^6) atom in Fe-porphyrin, and one would a priori expect a similar electronic structure. An early spin-unrestricted DFT (BP86 functional) study of the electronic structure of unsubstituted Co-corrole confirmed that the electronic ground state indeed also has intermediate-spin state (S = 1), corresponding to an electronic configuration $(d_{x^2-y^2})^2(d_{z^2})^2(d_{xz},d_{yz})^2$.[93] A low-lying singlet state is found at 0.26 eV, whereas the lowest quintet state is calculated at 1.08 eV. All three states were found to have the same (+3) oxidation state on cobalt. The lowest singlet state is an open-shell state corresponding to the same configuration as the triplet ground state (cf. the lowest singlet state in iron porphin; see previous section). However, unlike iron porphin, the lowest quintet state is in Co-corrole much higher-lying and does not correspond to a Co(III) high-spin configuration. Instead, a $\pi \rightarrow \pi^*$ transition is found to give rise to the lowest quintet excited state. That the σ antibonding $3d_{xy}$ orbital does not easily become occupied in Co-corrole may be explained by the rigid trianionic-ligand framework of corrolate, with a smaller cavity and corresponding stronger σ donation than the porphinate ligand in Fe-porphin.

In this work we report the results obtained from a comparative CASPT2 versus RASPT2 study of the ground state and a selected set of low-lying excited states of unsubsituted cobalt corrole, denoted as Co(C) (see Figure 2 for the structure (C_{2v}) and orientation of the axes). For the ground state, both CASPT2 and RASPT2 confirm the previous DFT prediction of a triplet Co(III) state $^3B_1$ with an electronic configuration of $(d_{x^2-y^2})^2(d_{z^2})^2(d_{xz})^1(d_{yz})^1$. Rather than considering other Co(III) states we have focused here on the possible occurrence of low-lying Co(II)-$(C)^{\bullet 2-}$ radical states. Starting from the $^3B_1$ ground state, we have considered excitations out of the two highest corrolate π orbitals of symmetry a_2 and b_2 into the cobalt $3d_{xz}$ orbital, giving rise to either ferro- or antiferromagnetic coupling between the remaining singly occupied cobalt $3d_{yz}$ orbital (residing in the representation a_2) and an a_2 or b_2 corrole π-radical. Of course, other low-lying Co(II) states, corresponding to different $(d_{x^2-y^2})^2(d_{xz},d_{yz},d_{z^2})^5(C)\pi^1$ arrangements, are also possible. A more complete description of the Co(C) spectrum will be provided in a separate paper.

3.5.1. Computational Details. Single point CASPT2/RASPT2 calculations were performed on structures obtained from DFT (in its unrestricted formalism, employing the PBE0 functional) using TZVP basis sets on all atoms. C_{2v} symmetry was maintained in all geometry optimizations. For conformity with iron porphin (previous section) the molecule was placed in the xy-plane with the x-axis as the C_2 axis (Figure 1).

Table 7. Relative Energy (eV) of Selected Low-Lying Triplet Electronic States of Co(C) with Respect to the $^3B_1$ Ground State. [a]

	CASPT2	SD	SDT	SDTQ	full CI
CI based on CASSCF orbitals					
			RASPT2(12,*l*,*m*;4,4,6)		
$^3B_1((d_{yz})^1(b_2)^1)$	0.29	0.43	0.37	0.36	0.36
$^3A_1((d_{yz})^1(a_2)^1)$	0.78	0.95	0.88	0.87	0.86
			RASPT2(12,*l*,*m*;2,6,6)		
$^3B_1((d_{yz})^1(b_2)^1)$	0.29	0.36	0.29	0.28	0.28
$^3A_1((d_{yz})^1(a_2)^1)$	0.78	0.88	0.80	0.78	0.78
			RASPT2(12,0,m;0,8,6)		
$^3B_1((d_{yz})^1(b_2)^1)$	0.29	0.35	0.29	0.28	0.28
$^3A_1((d_{yz})^1(a_2)^1)$	0.78	0.87	0.79	0.78	0.78
CI based on RASSCF/SD orbitals					
			RASPT2(12,*l*,*m*;4,4,6)		
$^3B_1((d_{yz})^1(b_2)^1)$	0.29	0.42	0.37	0.36	0.36
$^3A_1((d_{yz})^1(a_2)^1)$	0.82	0.98	0.92	0.90	0.90
			RASPT2(12,*l*,*m*;2,6,6)		
$^3B_1((d_{yz})^1(b_2)^1)$	0.33	0.38	0.32	0.31	0.31
$^3A_1((d_{yz})^1(a_2)^1)$	0.85	0.92	0.85	0.84	0.84
			RASPT2(12,0,m;0,8,6)		
$^3B_1((d_{yz})^1(b_2)^1)$	0.33	0.37	0.32	0.31	0.31
$^3A_1((d_{yz})^1(a_2)^1)$	0.85	0.91	0.85	0.84	0.84

[a] Single point CASSCF/CASPT2 and RASSCF/RASPT2 (CI only) calculations.

The active space used in the CASSCF/CASPT2 calculations was constructed similarly as for the iron porphin presented in the previous section, i.e., with eight electrons distributed over the cobalt 3d, 3d′, and the bonding σ(Co−N) orbital. However, since the $3d_{xy}$ orbital is in this case unoccupied in all considered states, its correlating $3d'_{xy}$ orbital was not included. This gives a CAS(8,10) space. On top of this, to consider also Co(II)-$(C)^{\bullet 2-}$ radical states the two highest-occupied π orbitals of the corrole (a_2, b_2) and their correlating π^* orbitals were made active, leading to a CAS(12,14) space.

RASPT2 calculations were performed with three global active spaces: the original (12,14) space and two larger spaces, constructed by extending this (12,14) space either with all or with a selection of the remaining corrole π and π^* orbitals, giving respectively a RAS(34,33) or RAS(26,25) space. The latter active space lacks the four occupied corrole π and their four correlating π^* orbitals built as combinations of the $2p_\pi$ orbitals of the eight β carbons of the corrole rings (a plot of these orbitals can be found in the Supporting Information). A similar active space was employed in a recent RASPT2 study of the iron-oxo porphyrins $FeO(P)^+$ and FeO(P)Cl.[10] The presence of an axial oxo ligand in these complexes put higher demands on the size of the RAS2 space (which has to contain the six orbitals involved in the very covalent FeO bond), thus precluding the use of a RAS space including all porphin π and π^* orbitals. The present test calculations with the smaller RAS(26,25) therefore serve as a (additional) check for the quality obtained from the RASPT2 calculations on these iron-oxo systems.

For the Co(C) calculations in this work, three different subpartitions of the global RAS space were considered. In all three cases, the four Co 3d′ orbitals and all active π^* orbitals were collected in RAS3, which thus consists of 6 orbitals in all RAS(12,14) calculations, 10 orbitals in all RAS(26,25) calculations, and 14 orbitals in all RAS(34,33) calculations. Also, the two singly occupied orbitals in each of the open-shell Co(II) π-radical cation states were systematically put in RAS2, thus avoiding the strict need of including up-to-triple excitations out of RAS1 and into RAS3, which would become computationally too demanding for the two largest active spaces. Next to these two state-specific orbitals, the smallest RAS2 space only contains the bonding and antibonding orbitals involved in the covalent Co $3d_{xy}$−corrole σ interaction. The second option for RAS2 is to include all four orbitals that become singly occupied in any of the five considered states, i.e., corrole π HOMO (a_2, b_2), and the cobalt $3d_{xz}$, $3d_{yz}$ orbitals. Adding also the (σ,σ^*) couple gives a six-orbital RAS2. The largest RAS2 considered includes on top of this the two remaining, doubly occupied, Co $3d_{z^2}$, $3d_{x^2-y^2}$ orbitals.

3.5.2. Results and Discussion. A first series of RASPT2 calculations was performed based on the (12,14) active space, and considering only triplet states: the Co(III) ground state $^3B_1((d_{xz})^1(d_{yz})^1)$ and the two excited states $^3B_1$, $^3A_1$ with configuration $((d_{xz})^2(d_{yz})^1)$ on Co(II) coupled ferromagnetically to either a corrole b_2 or a_2 π radical. The goal of these smaller calculations is two-fold: (a) to explore the minimum size of the RASSCF reference wave function that would be needed to obtain an accuracy which is close to the parent CASPT2 result, by systematically varying the size of RAS2 and the excitation level *l*, *m*, and (b) to investigate the effect of the optimization level of the active orbitals on the relative energies obtained from CASPT2/RASPT2. A similar exercise was already performed for CrF_6 in Section 3.1. Here, we decided to investigate this point further by comparing the results from two sets of CASPT2 and RASPT2 calculations, starting from reference wave functions in which only the CI coefficients are optimized (allowing up to full CI) but making use of orbitals obtained from either the full CAS(12,14) calculation or from the corresponding RAS(12,2,2;4,4,6), RAS(12,2,2;2,6,6), or RAS(12,0,2;0,8,6) calculation. The results of these RASPT2(12,14) calculations are shown in Table 7. As can be seen from this table, the differences between the calculated relative energies with the two sets of orbitals are relatively small, 0.06 eV or less. This further confirms that RASSCF orbitals obtained from an SD calculation may rather safely be used to obtain reference wave functions with a higher excitation level, without a strict need for further (time-consuming and generally poorly convergent) orbital optimizations.

Turning next to the different excitation levels in Table 7, we first note that the full CI reference wave function of the RASPT2 results shown in the rightmost column of this table is equal to the CASSCF wave function giving rise to the CASPT2 data in the leftmost column (i.e., both wave functions are built from the same orbitals and contain exactly the same number of configuration state functions). Any difference between both sets of results therefore should be traced back to the different perturbational treatment and more specifically to the neglect in RASPT2 of the off-diagonal Fock matrix elements connecting active orbitals belonging to different RAS subspaces. For a more detailed discussion of this phenomenon, see Section 3.2.

Table 8. Relative Energy (eV) of Selected Low-Lying Electronic States of Co(C) with Respect to the $^3B_1$ Ground State

	$^3B_1((d_{yz})^1(b_2)^1)$	$^1B_1((d_{yz})^1(b_2)^1)$	$^1A_1((d_{yz})^1(a_2)^1)$	$^3A_1((d_{yz})^1(a_2)^1)$
CASPT2(12,14)	0.29	0.29	0.43	0.78
RASPT2(12,2,2;4,4,6)	0.42	0.39	0.67	0.98
RASPT2(12,3,3;4,4,6)	0.37	0.34	0.60	0.92
RASPT2(12,2,2;2,6,6)	0.38	0.35	0.61	0.92
RASPT2(12,3,3;2,6,6)	0.32	0.29	0.53	0.85
RASPT2(26,2,2;11,4,10)	0.61	0.63	0.70	0.90
RASPT2(26,3,3;11,4,10)	0.60	0.62	0.69	0.89
RASPT2(26,2,2;9,6,10)	0.61	0.63	0.65	0.86
RASPT2(26,3,3;9,6,10)	0.58	0.60	0.59	0.81
RASPT2(34,2,2;15,4,14)	0.60	0.62	0.63	0.80
RASPT2(34,2,2;13,6,14)	0.67	0.70	0.69	0.86

The differences between the RASPT2 allowing up to full CI and CASPT2 results are significant, 0.07−0.08 eV, only for the calculations with the smallest RAS2, where the two sets of orbitals ($3d_{xz}$, $3d_{yz}$) and the corrole π HOMO orbitals of the same symmetry (b_2, a_2) are divided over RAS1 and RAS2. After including both sets of orbitals in RAS2, the RASPT2 calculations almost exactly converge (with increasing excitation level) to the CASPT2 results. The differences between the RASPT2 results obtained with the six- and eight-orbital RAS2 (the latter containing two extra cobalt 3d orbitals) are insignificantly small at all excitation levels. With these two RAS2 spaces, the difference between the CASSCF (or full CI) and the more limited RASSCF wave functions essentially comes down to a less complete description of the 3d double-shell effect and of corrole $\pi-\pi^*$ correlation in the latter wave function. As can be seen, up-to-triple RAS2 → RAS3 excitation is necessary but sufficient to bring the RASPT2 results to within 0.02 eV of the corresponding full CI RASPT2 results. The difference between the SD and full CI results is of the order of 0.1 eV. Differences of the same order of magnitude were also found for the energy differences between different (d^6) spin states in Fe(P) (Section 3.4), and will also be met in the next section, when trying to describe the relative energy of different low-lying states in FeO and FeO^-.

From the results in Table 7, it may therefore be concluded that it takes a six-orbital RAS2 combined with SDT excitations to obtain RASPT2 results that essentially match CASPT2. Unfortunately, the combination of these two conditions gives rise to very large RASSCF wave functions when extending the size of the global RAS space to more than twenty or so orbitals.

In Table 8 we compare the RASPT2 results obtained with the three global RAS spaces for both the ferromagnetic $^3B_1$ and $^3A_1$ and antiferromagnetic $^1B_1$ and $^1A_1$ Co(II)$(C)^{\bullet 2-}$ states. Both the four- and six-orbital RAS2 were used, allowing up-to-triple excitations for the two smallest RAS spaces but only up-to-doubles for the largest global RAS space. Comparing first the data with the two largest RAS spaces, we find differences of at most 0.1 eV between the numbers obtained with the same RAS2. The effect of triples is, for the global RAS(26,25) space, of the same order of magnitude, around 0.05 eV. On the whole, the combination of all data collected in both tables for Co(C) indicate that, for complicated electronic situations, such as the present cobalt corrole system with its different metal oxidation states in an extended π-delocalized ligand system, computational limitations still prevent the full exploitation of the possibilities of RASPT2, and the compromises that have to be made in the construction of the RAS space may lead to errors of around 0.2 eV.

This, however, does not alter the fact that very valuable results may be obtained with this method, pointing to deficiencies in the CASPT2 method that are the result of too limited active spaces. Two such deficiencies are eminent from the results in Table 8. First, from a comparison between the results obtained with the (12,14) and the more extended active spaces, it is clear that the relative energy of the a_2 versus b_2 π-radical states is not well described when including in the active space only the 'Gouterman' set of two π and two π^* orbitals. The energy of the $^{3,1}A_1$ (a_2 radical) states remains virtually constant when extending the active space with extra π orbitals. However, the $^{3,1}B_1$ states (b_2 radical) are quite strongly (about 0.25 eV) shifted upward in the RASPT2 calculations with more extended active spaces. We believe that this failure of CASPT2 to correctly reproduce the splitting between the a_2 and b_2 radical states should be brought back to an unbalanced treatment of corrole $\pi-\pi^*$ correlation when only four π orbitals are active. In the Co(III) ground state, all π orbitals are doubly occupied, and those two (π,π^*) pairs that give rise to the largest correlation energy enter the active space. However, these are not (necessarily) also the HOMO π orbitals, i.e., the ones that are most easily depopulated and therefore become active in the open-shell π-radical states. A plot of the four active corrole π orbitals in the CAS(12,14) treatment of the three triplet states is presented in Figure 3. One can see that these orbitals indeed quite strongly change shape between the different states considered.

A second failure of CASPT2 concerns the description of the magnetic coupling in the Co(II) π-radical states. Two cases should be distinguished here. In the $^{3,1}B_1$ states, the coupling occurs between two electrons residing in orbitals that are mutually orthogonal: $b_2(d_{xz})$ and $a_2(\pi)$. As the orbitals are strictly orthogonal, the coupling should be weakly ferromagnetic. As can be seen from Table 8, this is corroborated by the RASPT2(26,25) and RASPT2(34,33) results, with the $^3B_1$ state lying below $^1B_1$ by 0.02−0.03 eV. On the other hand, making use of the smaller (12,14) space, both CASPT2 and RASPT2 incorrectly predict the coupling to be weakly antiferromagnetic. In the second case, the a_2 π-radical states $^{3,1}A_1$, the interaction occurs between two orbitals that are weakly overlapping. As such, antiferromagnetic coupling is expected and confirmed by all results in Table 8. However, here the absolute value of the magnetic coupling is overestimated quite strongly with CASPT2, predicting a $^3A_1-{}^1A_1$ energy gap of more than 0.3 eV. This gap is decreased to 0.2 eV or less when extending the active space with extra corrole π^* orbitals.

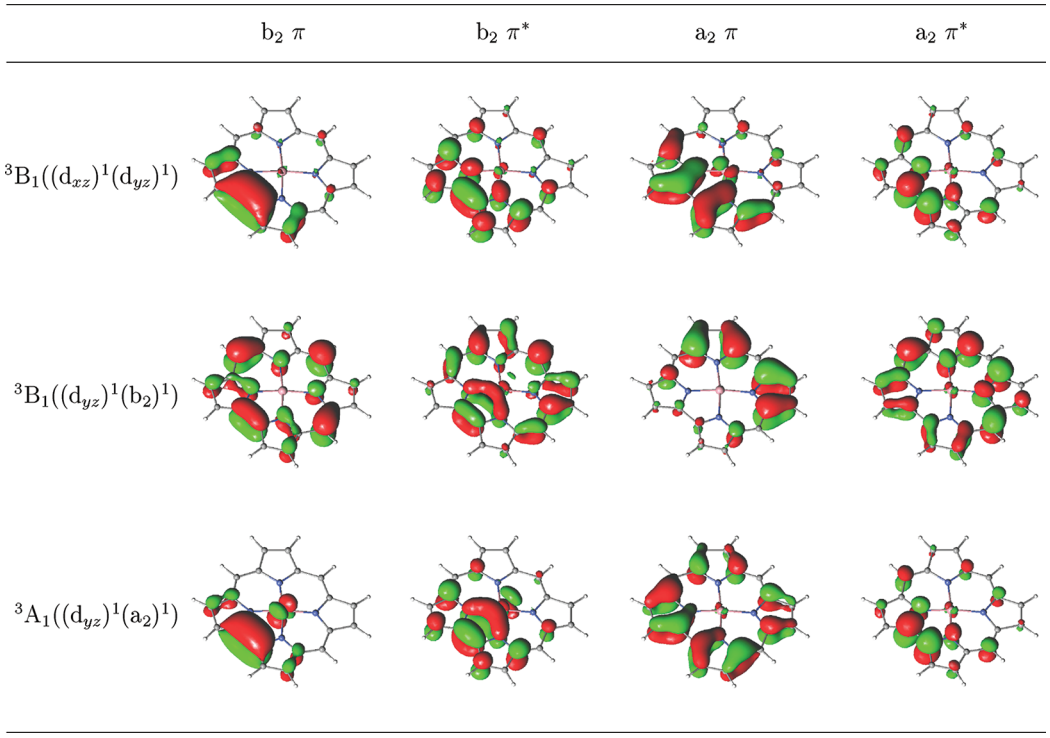

Figure 3. Four HOMO−LUMO π orbitals (as obtained from the CAS(12,14) calculations) for the selected triplet Co(Cor) states. The contour values are ± 0.04 e/au^3.

As a final note, we should also mention that the same two obvious failures of CASPT2 were already observed before when describing the relative energy of different electromers of copper corroles[9] and of iron−oxo porphyrins.[10] Obviously, even with its non-negligible error bars, the RASPT2 method has clear advantages over standard CASPT2 calculations also for these complicated cases.

3.6. Double-Shell Effects in the Low-Lying States of FeO and FeO$^-$. The iron−oxygen bond constitutes an important aspect of biological transportation and catalysis. This has been the prime motivation for many experimental and theoretical studies about the electronic structures of small iron oxides clusters in the gas phase.[23,94−100] The electronic structure of iron monoxide and its singly charged anion is particularly challenging because of the high density of low-lying states in both systems.[23,100] A theoretical multiconfigurational approach based on the CASPT2 method was used only recently to describe the electronic structure of FeO/FeO$^-$ and to provide an interpretation of the photoelectron spectrum of the anion starting from a $^6\Sigma^+$ ground state.[23] However, this CASPT2 assignment was shown to contradict the high-resolution autodetachment spectrum of FeO$^-$ which indicates that rather the $^4\Delta$ state is the ground state of the anion.[100] In a very recent ab initio study, high-level single-reference (RCCSD(T)) and multireference (MRCI) results were presented, confirming the CASPT2 prediction that the $^6\Sigma^+$ state is situated below the $^4\Delta$ state.[101] However, as the calculated energy difference between both states is extremely small (0.05 eV with R-CCSD(T), including Fe (3s,3p) correlation and scalar relativistic effects), it is proposed that $^6\Sigma^+$ could be embedded in the SOC components of $^4\Delta$.

In a qualitative orbital scheme for FeO the oxygen 2p orbitals give rise to bonding doubly occupied molecular orbitals, while the remaining six valence electrons are distributed among the predominantly iron 3d and 4s orbitals. Of these, the two lowest lying levels, 9σ and 1δ, are nonbonding, while the higher-lying 4π orbitals and in particular the 10σ orbital are antibonding. Occupying all six valence orbitals by one electron with parallel spin results in a $^7\Sigma^+$ ($9\sigma^1 1\delta^2 4\pi^2 10\sigma^1$) state. By transferring an electron from the most strongly antibonding 10σ orbital to the nonbonding 9σ or 1δ levels the $^5\Sigma^+$ ($9\sigma^2 1\delta^2 4\pi^2 10\sigma^0$) and $^5\Delta$ ($9\sigma^1 1\delta^3 4\pi^2 10\sigma^0$) states are reached. The latter state is generally considered as the ground state of FeO. For the corresponding FeO$^-$ anion, this orbital picture leads to three possible low-lying electronic states obtained by placing the extra electron in one of the nonbonding orbitals 9σ or 1δ. Starting from the neutral $^7\Sigma^+$ state, this gives $^6\Sigma^+$ ($9\sigma^2 1\delta^2 4\pi^2 10\sigma^1$) or $^6\Delta$ ($9\sigma^1 1\delta^3 4\pi^2 10\sigma^1$) states, while both quintets may accept the extra electron to form the same low-lying $^4\Delta$ ($9\sigma^2 1\delta^3 4\pi^2 10\sigma^0$) state.

The original CASPT2 calculations[23] were performed with an active space of 14 orbitals, consisting of nine valence orbitals O 2p, Fe (3d,4s) and extended with five virtual orbitals of σ, π, δ symmetry. Although initially intended to describe the Fe 3d double-shell effect, the extra σ, π orbitals turned out to have strongly mixed Fe 3d/O 3p character, the latter even providing the most dominant contribution. A more balanced description should include both the double-shell effect on iron and the oxygen anion. This would then give rise to an active space of 17 orbitals, accommodating either 12 (FeO) or 13 (FeO$^-$) electrons. CASPT2 calculations with such a large active space are computationally expensive, in particular if they have to be combined with the optimization of geometrical parameters. Therefore we decided to investigate instead the possibilities of RASPT2, using an active space in which the double-shell effect on both atoms is described by an active space with the appropriate correlating orbitals placed in the RAS3 subspace. Moreover, given the option for a larger active space in RASSCF, we also chose to include

Table 9. Fe−O Bond Distance (Å) and Relative Energy (eV) with Respect to the $^6\Sigma^+$ state of FeO^- of the Different Electronic States of FeO and FeO^-

	FeO^-			FeO		
	$^4\Delta$	$^6\Sigma^+$	$^6\Delta$	$^5\Delta$	$^5\Sigma^+$	$^7\Sigma^+$
Fe−O Bond Distance (Å)						
CASPT2(12/13,14)[a]	1.634	1.683	1.688	1.612	1.626	1.677
RASPT2(14/15,0,2;0,10,19)	1.619	1.677	1.673	1.611	1.620	1.671
Relative Energy (eV)						
CASPT2(12/13,14)[a]	0.13	0.00	0.36	1.51	1.55	1.75
RASPT2(14/15,0,2;0,10,9)	0.04	0.00	0.29	1.24	1.32	1.64
RASPT2(14/15,0,3;0,10,9)	0.01	0.00	0.34	1.33	1.41	1.73
RASPT2(14/15,0,4;0,10,9)	0.02	0.00	0.23	1.39	1.48	1.77
RASPT2(14/15,0,5;0,10,9)	0.02	0.00	0.23	1.40	1.49	1.78
RASPT2(14/15,0,6;0,10,9)	0.02	0.00	0.23	1.40	1.49	1.78

[a] From Hendrickx and Anam,[23] CASPT2 results obtained with ANO-rcc basis sets contracted to Fe[8s7p6d4f2g1h] O[7s6p4d3f1g], except for the $^6\Delta$ state, for which only results with a smaller contraction Fe-[8s7p5d4f2g] and O[6s5p4d2f] were reported.

the O (2s,3s) shells, thus obtaining a RAS(14/15,0,m;0,10,9) including all FeO valence orbitals in RAS2 and their correlating shells in RAS3. Calculations with an excitation level $m = 2-6$ were performed.

The molecular orbitals and the Fe−O bond distance were optimized only for the SD calculations, while single-point CI calculations were performed for the higher excitation levels, employing the orbitals and Fe−O distances from the optimized SD calculations. Calculations were performed with ANO-rcc basis sets,[25,26] using a very extended contraction scheme: [10s9p8d6f4g2h] for iron and [8s7p4d3f2g] on O. The results obtained from this work are presented in Table 9, where they are compared to the results from our previous CASPT2 study.[23]

Considering first the calculated Fe−O bond distances, one can observe a significant bond shortening when going from CASPT2 to RASPT2. The largest differences, 0.015 Å, are found for the FeO^- $^4\Delta$, $^6\Delta$ states. The Fe−O distances obtained from RASPT2 show a very clear pattern: Very similar distances, 1.671−1.677 Å, are obtained for the high-spin states of both molecules, whereas the calculated distances for all low-spin states are considerably shorter, 1.611−1.620 Å, but also these values differ by less than 0.01 Å among themselves. The reason for this observation lies in the occupation of the strongly antibonding 10σ orbital in the high-spin states, and the fact that among themselves, both the low- and high-spin states only differ in the occupation of the 9σ and 1δ nonbonding orbitals. A similar pattern is also found at the CASPT2 level, although the differences are here somewhat larger.

Table 9 also shows that the different low-lying states of FeO and FeO^- are indeed close in energy, lying within a range of 0.4 eV for each of the methods used. For FeO, all calculations confirm the generally accepted assignment of a $^5\Delta$ ground state. At the CASPT2 level the $^6\Sigma^+$ state was calculated as the ground state of FeO^-. This assignment was, however, disputed[100] based on its experimental autodetachment spectrum,[94] showing a fully rotationally resolved fine structure that can only originate from a ground state with the spin−orbit fine structure characteristic of a $^4\Delta$ state. As one can see from Table 9, the energy difference between the two candidate ground states of FeO^- is substantially reduced when introducing a more complete description of the double-shell effect in the RASPT2 calculation. A similar trend is found for all other low-spin states, which are all stabilized by around 0.1 eV in RASPT2 as compared to CASPT2. On the other hand, the relative energy between the two high-spin states, $^7\Sigma^+ - {}^6\Sigma^+$ is slighly higher with RASPT2(SDTQ) than with CASPT2. Convergence of the RASPT2 results is essentially reached at the SDTQ level. It should be noted though that the differences between the lower excitation levels in RASPT2 are quite significant, up to 0.16 eV between SD and SDTQ, and show oscillating behavior with the excitation level in case of the $^6\Delta$ state. Similar (although generally smaller) errors in the RASPT2-(SD) description of the Fe 3d double-shell effect were already met in case of Fe(P) (Table 6). It should be clear from these and other RASPT2 results in this work (e.g., the test results for Co(C) in Tables 7 and 8) that uncertainties of 0.1−0.2 eV on relative energies are to be expected from RASPT2 when limiting the excitation levels out of RAS1 and into RAS3 to only SD. Such error bars become particularly bothersome when trying to describe the relative energy of close-lying states, as is the case here.

An important observation from the results in Table 9 is also that the two states $^4\Delta$ and $^6\Sigma^+$ in FeO^- are very nearly degenerate. It is quite probable that, when including SOC in the calculations, the actual ground state of FeO^- might in fact become a mixture of both states, with an Fe−O distance which is intermediate between the calculated distances of 1.619 Å for the $^4\Delta$ and 1.677 Å for the $^6\Sigma^+$ states. Such a mixed ground state is in fact suggested by the experimental Fe−O bond length of 1.641 Å (derived from the experimental rotational constant for the $\Omega = 7/2$ ground state observed in the autodetachment spectrum) and will be further investigated in a separate study, by performing relativistic RASPT2 geometry optimizations, including SOC for all low-lying states of FeO^-.

4. SUMMARY AND CONCLUSIONS

In this work we have presented the results of an explorative study of different properties of a series of six representative first-row TM systems by means of the recently introduced RASPT2 method.[4] Different RASPT2 strategies were investigated for each molecule, aimed at obtaining the highest possible accuracy to be reached by a multiconfigurational perturbation theory method at the lowest possible computational cost. This was accomplished by a two-step procedure, starting first with a series of calculations with a 'standard' active space, containing the most important correlation effects (3d double-shell and/or correlation effects connected to covalent TM−ligand interactions) but with a size which is small enough to be tractable by CASPT2. In this series of calculations, different RAS subpartitions and excitation levels were explored, aiming at keeping the accuracy of the RASPT2 results as close as possible to CASPT2, while reducing the number of configuration-state functions in the reference wave function. From these calculations, the following general rules for the construction of RAS spaces may be formulated:

(a) In case of covalent metal−ligand interactions all bonding−antibonding orbital pairs between the ligands and the metal 3d orbitals should be kept together in RAS2, in order to allow full rotational freedom between these orbital pairs in the diagonalization of the active part of the Fock matrix.

(b) The 3d double-shell effect may be adequately described by putting the second 3d′ shell in RAS3. However, in order to avoid errors of the order of 0.1 eV (a few kcal/mol) at least up-to-triple excitations into RAS3 might be necessary in many cases, such as the description of spin state energetics (in Fe(P)), charge-transfer states (in Co(C)), etc. (see also the cases of Ni and $CuCl_4^{2-}$ in a previous RASPT2 study[6]). In cases where combined double-shell effects are described by means of RASSCF, such as the case of FeO in the present work (see also the binuclear copper compounds described previously)[4] up-to-quadruple excitations into RAS3 are necessary.

(c) Excitation processes may be described either by using a different RAS2 for each specific state, containing those orbital(s) that become singly occupied [on top of the covalent orbitals described in (a)] or by keeping such orbitals in either RAS1 or RAS3 but then allowing at least up-to-triples in or out of these subspaces, so as to describe the combined effect of excitation/correlation.

In a second step, extensions of the active space (either in RAS1 and RAS3 or both) were considered, aiming at increasing the accuracy of the RASPT2 results beyound the limits of CASPT2. For ferrocene and $Cr(CO)_6$, the additional orbitals served to provide a more complete description of the double-shell effect as well as correlation within the ligand π orbitals. Including these orbitals in the active space was shown to give a significant improvement of the results obtained from the perturbational treatment, bringing the RASPT2 result for the heterolytic binding energy of ferrocene (641.4 kcal/mol) within the error limits of the experimental value (641 ± 6 kcal/mol), and the RASPT2 excitation energies of the two allowed CT transitions in $Cr(CO)_6$ to within 0.1 eV of the experimental band maxima. For both molecules, this was accomplished by RASPT2(SD) after constructing the RAS space according to the rules given above. For CrF_6 it turned out that even with a 10-orbital RAS2 at least RASPT2(SDTQ) is necessary to obtain accurate results for the energy difference between the D_{3h} and O_h structures. This may not come as a surprise, given the very strong correlation effects in this molecule involving also excitations from nonbonding F 2p orbitals (in RAS1) into Cr 3d (in RAS2).[14] Nevertheless, also for CrF_6 the RASPT2 method offers a clear improvement over CASPT2, which is dramatically suffering from limitations in the size of the CAS space. For the two heme or heme-related systems Fe(P) and Co(C), the largest active spaces comprised the entire set of heme π orbitals. Including at least 15 corrole π orbitals rather than just a few frontier orbitals (such as the Gouterman set of two π and two π^* orbitals) is shown to give a considerable improvement of the RASPT2 results for the splitting between the a_2 and b_2 radicals on the corrole ligand and for the strength of the magnetic coupling in both types of Co(II) π-radical states. However, with an active space containing as much as 33 orbitals, combining an optimal RAS2 with RASPT2(SDT) becomes computationally unfeasible. Although the RASPT2 results are also for Co(C) superior to CASPT2, a larger error bar of 0.1−0.2 eV has to be accepted for such a difficult case. On the other hand, for Fe(P) including the (full set of) porphin π orbitals in the active space does not affect the spin state energetics of the different Fe(II) states to any significant extent. Here it is shown that including instead in the active space the Fe semicore (3s,3p) orbitals significantly improves the description of (3s,3p)−3d intershell correlation effects, thereby correctly reproducing the $^3A_{2g}$ state as the ground state of Fe(P). The (experimentally observed) high magnetic moment associated with this triplet state is correctly reproduced after introducing SOC in the CASPT2(16,15) calculations, thus allowing mixing of $^3A_{2g}$ with the close-lying $^5A_{1g}$ and ^3E_g states. Finally, for FeO^- the present RASPT2 results predict a quasidegenerate $^6\Sigma^+ - ^4\Delta$ ground state (the latter state situated at only 0.02 eV above the former). Also here, SOC may be expected to become crucial in correctly describing the structure and character of the ground state. A more detailed analysis of the low-lying states of FeO/FeO^- will be presented in a separate paper.

In conclusion, the results presented in this work have clearly illustrated the strength of the RASPT2 method for the prediction of several important properties in first-row TM systems, thus establishing this method as a valuable tool for studying large TM complexes with complicated electronic structures, creating the need for very large active spaces.

■ ASSOCIATED CONTENT

Supporting Information. Contour plots of the active orbitals included in the most extended active space of all molecules. Contour plots of the eight active orbitals that are included in the (34,33) active space of Co(C) but not in the (26,25) space. Results obtained from the calculations on Fe(C) including SOC. This material is available free of charge via the Internet at http://pubs.acs.org.

■ AUTHOR INFORMATION

Corresponding Author
*E-mail: kristin.pierloot@chem.kuleuven.be.

■ ACKNOWLEDGMENT

This investigation has been supported by grants from the Flemish Science Foundation (FWO) and from the Concerted Research Action of the Flemish Government (GOA).

■ REFERENCES

(1) Andersson, K.; Malmqvist, P.-Å.; Roos, B. O.; Sadlej, A. J.; Wolinski, K. *J. Phys. Chem.* **1990**, *94*, 5483–5488.
(2) Andersson, K.; Malmqvist, P.-Å.; Roos, B. O. *J. Chem. Phys.* **1992**, *96*, 1218–1226.
(3) Ghosh, A. *J. Biol. Inorg. Chem.* **2011**, *16*, 819–820.
(4) Malmqvist, P.-Å.; Pierloot, K.; Shahi, A. R. M.; Cramer, C. J.; Gagliardi, L. *J. Chem. Phys.* **2008**, *128*, 204109.
(5) Huber, S. M.; M.Shahi, A. R.; Aquilante, F.; Cramer, C.; L. Gagliardi *J. Chem. Theory Comput.* **2009**, *5*, 2967–2976.
(6) Sauri, V.; Serrano-Andrés, L.; Shahi, A. R. M.; Gagliardi, L.; Vancoillie, S.; Pierloot, K. *J. Chem. Theory Comput.* **2011**, *7*, 153–168.
(7) Ruipérez, F.; Aquilante, F.; Ugalde, J. M.; Infante, I. *J. Chem. Theory Comput.* **2011**, *7*, 1640–1646.
(8) Shahi, A. R. M.; Cramer, C. J.; Gagliardi, L. *Phys. Chem. Chem. Phys.* **2009**, *11*, 10964–10972.
(9) Pierloot, K.; Zhao, H.; Vancoillie, S. *Inorg. Chem.* **2010**, *49*, 10316–10329.
(10) Radoń, M.; Broclawik, E.; Pierloot, K. *J. Chem. Theory Comput.* **2011**, *7*, 898–908.
(11) Andersson, K.; Roos, B. O. *Chem. Phys. Lett.* **1992**, *191*, 507–514.
(12) Roos, B. O.; Andersson, K.; Fülscher, M. P.; Malmqvist, P.-Å.; Serrano-Andrés, L.; Pierloot, K.; Merchán, M. In *Advances in Chemical Physics:*

New Methods in Computational Quantum Mechanics; Prigogine, I., Rice, S. A., Eds.; John Wiley & Sons: New York, 1996; Vol. XCIII, pp 219−332.
(13) Pierloot, K. Nondynamic Correlation Effects in Transition Metal Coordination Compounds. In *Computational Organometallic Chemistry*; Cundari, T. R., Ed.; Marcel Dekker, Inc.: New York, 2001; pp 123−158.
(14) Pierloot, K. *Mol. Phys.* **2003**, *101*, 2083–2094.
(15) Pierloot, K. *Int. J. Quantum Chem.* **2011**, *111*, 3291–3301.
(16) Veryazov, V.; Malmqvist, P.; Roos, B. O. *Int. J. Quantum Chem.* **2011**, *111*, 3329–3338.
(17) Pierloot, K.; Roos, B. O. *Inorg. Chem.* **1992**, *31*, 5353–5354.
(18) Persson, B. J.; Roos, B. O.; Pierloot, K. *J. Chem. Phys.* **1994**, *101*, 6810–6821.
(19) Pierloot, K.; Persson, B. J.; Roos, B. O. *J. Phys. Chem.* **1995**, *99*, 3465–3472.
(20) Pierloot, K.; Tsokos, E.; Vanquickenborne, L. G. *J. Phys. Chem.* **1996**, *100*, 16545–16550.
(21) Radoń, M.; Pierloot, K. *J. Phys. Chem. A* **2008**, *112*, 11824–11832.
(22) Vancoillie, S.; Zhao, H.; Radoń, M.; Pierloot, K. *J. Chem. Theory Comput.* **2010**, *6*, 576–582.
(23) Hendrickx, M. F. A.; Anam, K. R. *J. Phys. Chem. A* **2009**, *113*, 8746–8753.
(24) Aquilante, F.; De Vico, L.; Ferré, N.; Ghigo, G.; Malmqvist, P.-Å.; Neogrády, P.; Pedersen, T. B.; Pitoňák, M.; Reiher, M.; Roos, B. O.; Serrano-Andrés, L.; Urban, M.; Veryazov, V.; Lindh, R. *J. Comput. Chem.* **2010**, *31*, 224–247.
(25) Roos, B. O.; Lindh, R.; Malmqvist, P.-Å.; Veryazov, V.; Widmark, P.-O. *J. Phys. Chem. A* **2004**, *108*, 2851–2858.
(26) Roos, B. O.; Lindh, R.; Malmqvist, P.-A.; Veryazov, V.; Widmark, P.-O. *J. Phys. Chem. A* **2005**, *109*, 6575–6579.
(27) Douglas, N.; Kroll, N. M. *Ann. Phys. (N. Y.)* **1974**, *82*, 89.
(28) Hess, B. *Phys. Rev. A* **1986**, *33*, 3742.
(29) Roos, B. O.; Malmqvist, P.-Å. *Phys. Chem. Chem. Phys.* **2004**, *6*, 2919–2927.
(30) Reiher, M.; Wolf, A. *J. Chem. Phys.* **2004**, *121*, 10945–10956.
(31) Ghigo, G.; Roos, B. O.; Malmqvist, P.-Å. *Chem. Phys. Lett.* **2004**, *396*, 142–149.
(32) Forsberg, N.; Malmqvist, P.-A. *Chem. Phys. Lett.* **1997**, *274*, 196.
(33) Aquilante, F.; Pedersen, T. B.; Lindh, R. *J. Chem. Phys.* **2007**, *126*, 194106.
(34) Aquilante, F.; Malmqvist, P.-Å.; Pedersen, T. B.; Ghosh, A.; Roos, B. O. *J. Chem. Theory Comput.* **2008**, *4*, 694.
(35) Aquilante, F.; Pedersen, T. B.; Lindh, R. *Theor. Chem. Acc.* **2009**, *124*, 1–10.
(36) Marsden, C. J.; Moncrieff, D.; Quelch, G. E. *J. Phys. Chem.* **1994**, *98*, 2038.
(37) Vanquickenborne, L. G.; Vinckier, A. E.; Pierloot, K. *Inorg. Chem.* **1996**, *35*, 1305–1309.
(38) Ryan, M. F.; Eyler, J. R.; Richardson, D. E. *J. Am. Chem. Soc.* **1992**, *114*, 8611–8619.
(39) Pierloot, K.; Dumez, B.; Widmark, P.-O.; Roos, B. O. *Theor. Chim. Acta* **1995**, *90*, 87–114.
(40) Klopper, W.; Luthi, H. P. *Chem. Phys. Lett.* **1996**, *262*, 546–552.
(41) Koch, H.; Jorgensen, P.; Helgaker, T. *J. Chem. Phys.* **1996**, *104*, 9528–9530.
(42) Haaland, A. *Top. Curr. Chem.* **1975**, *53*, 1.
(43) Beach, N. A.; Gray, H. B. *J. Am. Chem. Soc.* **1968**, *90*, 5713.
(44) Pollak, C.; Rosa, A.; Baerends, E. J. *J. Am. Chem. Soc.* **1997**, *119*, 7324–7329.
(45) Rosa, A.; Baerends, E.; van Gisbergen, S. J. A.; van Lenthe, A.; Groeneveld, J. A.; Snijders, J. G. *J. Am. Chem. Soc.* **1999**, *121*, 10356.
(46) Hummel, P.; Oxgaard, J.; Goddard, W. A., III; Gray, H. B. *Inorg. Chem.* **2005**, *44*, 2454–2458.
(47) Crespo-Otero, R.; Barbatti, M. *J. Chem. Phys.* **2011**, *134*, 164305.
(48) Ben Amor, N.; Villaume, S.; Maynau, D.; Daniel, C. *Chem. Phys. Lett.* **2006**, *421*, 378–382.
(49) Villaume, S.; Strich, A.; Daniel, C.; Perera, S. A.; Bartlett, R. J. *Phys. Chem. Chem. Phys.* **2007**, *9*, 6115–6122.
(50) Rees, B.; Mitschler, A. *J. Am. Chem. Soc.* **1976**, *98*, 7918.
(51) Finley, J.; Malmqvist, P.-Å.; Roos, B. O.; Serrano-Andrés, L. *Chem. Phys. Lett.* **1998**, *288*, 299–306.
(52) Collman, J. P.; Hoard, J. L.; Kim, N.; Lang, G.; Reed, C. A. *J. Am. Chem. Soc.* **1975**, *97*, 2676–2681.
(53) Goff, H.; La Mar, G. N.; Reed, C. A. *J. Am. Chem. Soc.* **1977**, *99*, 3641–3646.
(54) Kitagawa, T.; Teraoka, J. *Chem. Phys. Lett.* **1979**, *63*, 443–446.
(55) Dolphin, D.; Sams, J. R.; Tsin, T. B.; Wong, K. L. *J. Am. Chem. Soc.* **1976**, *98*, 6970–6975.
(56) Lang, G.; Spartalian, K.; Reed, C. A.; Collman, J. P. *J. Chem. Phys.* **1978**, *69*, 5424–5427.
(57) Boyd, P. D. W.; Buckingham, A. D.; McMecking, R. F.; Mitra, S. *Inorg. Chem.* **1979**, *18*, 3585–3591.
(58) Mispelter, J.; Momenteau, M.; Lhoste, J. M. *J. Chem. Phys.* **1980**, *72*, 1003–1012.
(59) Strauss, S. H.; Silver, M. E.; Long, K. M.; Thompson, R. G.; Hudgens, R. A.; Spartalian, K.; Ibers, J. A. *J. Am. Chem. Soc.* **1985**, *107*, 4207–4215.
(60) *Iron Porphyrin*; Lever, A. B. P., Gray, H. B., Eds. Addison-Wesley, Inc.: Reading, MA, 1983.
(61) Obara, S.; Kashiwagi, H. *J. Chem. Phys.* **1982**, *77*, 3155.
(62) Dedieu, A.; Rohmer, M.-M.; Veillard, A. *Adv. Quantum Chem.* **1982**, *16*, 43–95.
(63) Rawlings, D. C.; Gouterman, M.; Davidson, E.; Feller, D. *Int. J. Quantum Chem.* **1985**, *28*, 773–796.
(64) Kozlowski, P. M.; Spiro, T. G.; Bérces, A.; Zgierski, M. Z. *J. Phys. Chem. B* **1998**, *102*, 2603–2608.
(65) Choe, Y.-K.; Hashimoto, T.; Nakano, H.; Hirao, K. *Chem. Phys. Lett.* **1998**, *295*, 380–388.
(66) Choe, Y.-K.; Nakajima, T.; Hirao, K.; Lindh, R. *J. Chem. Phys.* **1999**, *111*, 3837–3844.
(67) Scherlis, D. A.; Estrin, D. A. *Int. J. Quantum Chem.* **2002**, *87*, 158–166.
(68) Liao, M.-S.; Scheiner, S. *J. Chem. Phys.* **2002**, *117*, 205–219.
(69) Deeth, R. J. *Struct. Bonding (Berlin, Ger.)* **2004**, *113*, 37–69.
(70) Deeth, R. J.; Fey, N. *J. Comput. Chem.* **2004**, *25*, 1840–1848.
(71) Groenhof, A. R.; Swart, M.; Ehlers, A. E.; Lammertsma, K. *J. Phys. Chem. A* **2005**, *109*, 3411–3417.
(72) Liao, M.-S.; Watts, J. D.; Huang, M.-J. *J. Phys. Chem. A* **2007**, *111*, 5927–5935.
(73) Khvostichenko, D.; Choi, A.; Boulatov, R. *J. Phys. Chem. A* **2008**, *112*, 3700–3711.
(74) Ahlrichs, R.; Bär, M.; Häser, M.; Horn, H.; Kölmel, C. *Chem. Phys. Lett.* **1989**, *162*, 165–169.
(75) Treutler, O.; Ahlrichs, R. *J. Chem. Phys.* **1995**, *102*, 346.
(76) Pierloot, K.; Tsokos, E.; Roos, B. O. *Chem. Phys. Lett.* **1993**, *214*, 583.
(77) Malmqvist, P. Å.; Roos, B. O.; Schimmelpfennig, B. *Chem. Phys. Lett.* **2002**, *357*, 230–240.
(78) Hess, B. A.; Marian, C. M.; Wahlgren, U.; Gropen, O. *Chem. Phys. Lett.* **1996**, *251*, 365–371.
(79) Christiansen, O.; Gauss, J.; Schimmelpfennig, B. *Phys. Chem. Chem. Phys.* **2000**, *2*, 965–971.
(80) Vahtras, O.; Engström, M.; Schimmelpfennig, B. *Chem. Phys. Lett.* **2002**, *351*, 424–430.
(81) Vancoillie, S.; Rulíšek, L.; Neese, F.; Pierloot, K. *J. Phys. Chem. A* **2009**, *113*, 6149–6157.
(82) Ghosh, A.; Wondimagegn, T.; Parusel, A. B. J. *J. Am. Chem. Soc.* **2000**, *122*, 5100–5104.
(83) Bröring, M.; Brégier, F.; Cónsul Tejero, E.; Hell, C.; Holthausen, M. C. *Angew. Chem., Int. Ed.* **2007**, *46*, 445–448.
(84) Paolesse, R.; Kadish, K. M.; Smith, K. M.; Guilard, R. *The Porphyrin Handbook*; Academic Press: Boston, MA, 2000; Vol. 2; pp 201−300.
(85) Paolesse, R. *SYNLETT* **2008**, *15*, 2215–2230.
(86) Grodkowski, J.; Neta, P.; Fujita, E.; Mahammed, A.; Simkhovich, L.; Gross, Z. *J. Phys. Chem. A* **2002**, *106*, 4772–4778.

(87) Will, S.; Lex, J.; Vogel, E.; Adamian, V. A.; Caemelbecke, E. V.; Kadish, K. M. *Inorg. Chem.* **1996**, *35*, 5577–5583.
(88) Guilard, R.; Gros, C. P.; Bolze, F.; Jérôme, F.; Ou, Z. P.; Shao, J. G.; Fischer, J.; Weiss, R.; Kadish, K. M. *Inorg. Chem.* **2001**, *40*, 4845.
(89) Kadish, K. M.; Ou, Z. P.; Shao, J. G.; Gros, C. P.; Barbe, J. M.; Jérôme, F.; Bolze, F.; Burdet, F.; Guilard, R. *Inorg. Chem.* **2002**, *41*, 3990.
(90) Maiti, N.; Lee, J.; Kwon, S. J.; Kwak, J.; Do, Y.; Churchill, D. G. *Polyhedron* **2006**, *25*, 1519–1530.
(91) Barbe, J. M.; Canard, G.; Brandés, S.; Guilard, R. *Angew. Chem.* **2005**, *117*, 3163–3166.
(92) Guilard, R.; Burdet, F.; Barbe, J. M.; Gros, C. P.; Espinosa, E.; Shao, J.; Ou, R.; Kadish, K. M. *Inorg. Chem.* **2005**, *44*, 3972–3983.
(93) Rovira, C.; Kunc, K.; Hutter, J.; Parrinello, M. *Inorg. Chem.* **2001**, *40*, 11–17.
(94) Andersen, T.; Lykke, K. R.; Neumark, D. M.; Lineberger, W. C. *J. Chem. Phys.* **1987**, *86*, 1858.
(95) Engelking, P. C.; Lineberger, W. C. *J. Chem. Phys.* **1977**, *66*, 5054.
(96) Cheung, A. S.-C.; Lee, N.; Lyrra, A. M.; Merer, A. J.; Taylor, A. W. *J. Mol. Spectrosc.* **1982**, *95*, 213.
(97) Fan, J.; Wang, L.-S. *J. Chem. Phys.* **1995**, *102*, 8714.
(98) Wu, H. B.; Desai, S. R.; Wang, L. S. *J. Am. Chem. Soc.* **1996**, *118*, 5296.
(99) Drechsler, G.; Boesl, U.; Bassmann, C.; Schlag, E. W. *J. Chem. Phys.* **1997**, *107*, 2284.
(100) Neumark, D. M.; Lineberger, W. C. *J. Phys. Chem. A* **2009**, *113*, 10588.
(101) Sakellaris, C. N.; Milliordos, E.; Mavridis, A. *J. Chem. Phys.* **2011**, *134*, 234308.